Universidade de Aveiro Departamento de Química
Ano 2017

Tânia Marisa da Costa Lima

Alterações funcionais e moleculares no músculo cardíaco e esquelético na remodelagem e remodelagem reversa na ICFEp

Molecular and functional changes in cardiac and skeletal muscle in HFpEF remodelling and reverse remodelling

Universidade de Aveiro Departamento de Química
Ano 2017

Tânia Marisa da Costa Lima

Alterações funcionais e moleculares no músculo cardíaco e esquelético na remodelagem e remodelagem reversa na ICFEp

Molecular and functional changes in cardiac and skeletal muscle in HFpEF remodelling and reverse remodelling

Dissertação apresentada à Universidade de Aveiro para cumprimento dos requisitos necessários à obtenção do grau de Mestre em Bioquímica, realizada sob a orientação científica das Doutoras Rita Ferreira, Professora auxiliar do Departamento de Química da Universidade de Aveiro e da Doutora Inês Falcão Pires, Professora auxiliar da Faculdade de Medicina da Universidade do Porto.

Dedico este trabalho aos meus pais.

o júri

presidente

Prof. Doutor Pedro Miguel Dimas Neves Domingues
Professor auxiliar com agregação, Universidade de Aveiro

Doutora Inês Maria Falcão Sousa Pires Marques
Professora auxiliar, Faculdade de Medicina da Universidade do Porto

Doutor David Rizo Roca
Investigador de Pós Doutoramento, Faculdade de Desporto da Universidade do Porto

agradecimentos

Ao Professor Doutor Adelino Leite Moreira, Diretor do Departamento de Fisiologia e Cirurgia Cardiotorácica do Centro de Investigação Médica da Faculdade de Medicina da Universidade do Porto, pela oportunidade para realizar o meu trabalho nesta instituição.

Um obrigado muito especial à Daniela Miranda, sem ela este trabalho não seria possível, mais do que orientadora foi uma amiga, sempre disponível para ajudar quer a nível profissional, quer a nível pessoal. Espero um dia poder retribuir tudo aquilo que fez por mim e acima de tudo deixá-la orgulhosa de mim. Terá sempre aqui uma amiga e uma pessoa que a admira muito, não só como investigadora mas também como a pessoa gentil e genuína que é.

Não posso deixar de agradecer a todo o Departamento de Fisiologia que desde o primeiro dia me acolheu de braços abertos e que sempre me apoiou. Pessoas deste departamento como a Patrícia Rodrigues, Cláudia Mendes e Glória Almeida sempre me ajudaram e fizeram com que a fisiologia fosse uma segunda casa para mim. À Patrícia não podia deixar de agradecer todos os conselhos, toda a ajuda e toda a amizade.

À Sofia Costa e à Raquel Videira um muito obrigado por todos os conselhos, por todo o apoio, pela amizade, pelas conversas de café, certamente este ano sem vocês não teria sido o mesmo.

À Professora Doutora Inês Pires agradeço a oportunidade e o privilégio que tive em realizar a minha dissertação de mestrado no Departamento de Fisiologia, que muito contribuiu para o meu enriquecimento científico e pessoal.

À Professora Doutora Rita Ferreira um muito obrigado por todo o apoio, todos os conselhos, toda a disponibilidade sempre demonstrada. Sem si a realização desta tese não seria possível.

Aos meus pais e ao meu irmão o meu sincero obrigado, obrigado por sempre acreditarem em mim e nas minhas capacidades, mesmo quando muitas vezes eu própria duvidava delas. Foram o meu alicerce não só nesta etapa, como em todas, estando sempre presentes nos momentos mais difíceis, apoiando-me incondicionalmente, mas também nas minhas conquistas. Espero um dia conseguir retribuir de alguma forma tudo aquilo que me proporcionaram todos estes anos, espero que estejam orgulhosos de mim. Obrigado por todos os conselhos e especialmente por sempre me ensinarem que a humildade e o esforço são qualidades essenciais para o sucesso, porque esses valores estão sempre presentes na minha vida. A eles dedico este trabalho.

PALAVRA-CHAVE: Disfunção diastólica; intolerância ao exercício; reserva energética; alterações metabólicas; metabolismo; mitocôndria; *stress* oxidativo; apoptose; Remodelagem Reversa;

RESUMO: A insuficiência cardíaca (IC) com fração de ejeção preservada (ICFEp) é uma síndrome com uma etiologia muito diversificada, cuja disfunção metabólica tem sido apontada como um importante mecanismo associado à sua severidade. A remodelagem do miocárdio, resulta de uma agressão ao coração que pode ser direta (isquemia, estenose aórtica, etc) ou indireta (diabetes, disfunção renal, etc). Quando esta agressão é atenuada, por tratamento farmacológico ou cirúrgico, o coração sofre uma remodelagem reversa (RR) e o miocárdio retoma à sua estrutura e função normais. Conhecer os mecanismos subjacentes ao padrão de remodelagem e RR do miocárdio irá certamente potenciar novas oportunidades de tratamento da ICFEp. Por ser uma síndrome multisistémica, os doentes com ICFEp apresentam frequentemente sinais e sintomas extra-cardíacos característicos do diagnóstico desta patologia, como é o caso da intolerância ao esforço. Assim este trabalho teve como objetivos implementar e caracterizar um modelo animal de ICFEp, bem como avaliar as alterações estruturais, funcionais e moleculares que ocorrem ao nível do músculo cardíaco e esquelético na remodelagem e RR. Os nossos resultados mostram que a implementação de um modelo animal que mimetiza o fenótipo de ICFEp foi bem-sucedida. De facto, os animais *banding* apresentaram uma marcada hipertrofia do ventrículo esquerdo (VE), disfunção diastólica com rigidez do miocárdio, alterações na regulação do cálcio e aumento do *stress* oxidativo. Observaram-se ainda alterações que sugerem um aumento da biogénese e da fissão mitocondrial bem como um aumento dos transportadores de glucose. Apesar do aumento da expressão da proteína desacopladora 1 (UCP-1), funcionalmente, as mitocôndrias apresentaram uma melhoria da sua função. A redução da performance física dos animais *banding* foi acompanhada de alterações estruturais ao nível do músculo-esquelético, assim como de uma alteração dos transportadores dos substratos metabólicos. Curiosamente, nos animais *debanding*, apesar da recuperação funcional, morfologicamente o miocárdio não normalizou totalmente. Adicionalmente, observou-se um aumento dos transportadores de ácidos gordos, acompanhado por uma diminuição do *stress* oxidativo e da apoptose no VE. Além disso, apesar da melhoria metabólica, as mitocôndrias do VE dos animais *debanding* mantém-se menores. Relativamente à capacidade aeróbica dos animais, observou-se uma melhoria após o *debanding* acompanhada por uma reversão da atrofia e a fibrose das fibras musculares, assim como da oxidação dos ácidos gordos. Este trabalho mostra evidências do envolvimento mitocondrial e metabólico na progressão da ICFEp, ao nível dos músculo-esquelético e cardíaco.

KEYWORDS: Diastolic dysfunction; exercise intolerance; energetic reserve; metabolism abnormalities; cardiac metabolism; mitochondria; oxidative *stress*; apoptosis

ABSTRACT: Heart failure (HF) with preserved ejection fraction (HFpEF) is a complex syndrome with a diverse aetiology in which the metabolic dysfunction has been pointed out as an important mechanism that underlies the disease severity. Myocardial remodelling results from cardiac injury that can be direct (ischemia, aortic stenosis, etc) or indirect (diabetes, renal dysfunction, etc). When the deleterious stimulus is attenuated by pharmacological or surgical treatment, the heart enrols in a process called reverse remodelling (RR), and myocardial structure and function returns to normal. The knowledge of the molecular mechanism that underlie the RR process could represent an opportunity to develop novel therapeutic approaches and thus improve the treatment of HFpEF patients. As being a multi-systemic syndrome, HFpEF presents several extra-cardiac signals and symptoms typical of its diagnosis, such as effort intolerance. Thus, the aims of this work was to implement and characterize an animal model of cardiac remodelling and reverse remodelling of HFpEF and thus characterize structurally, functionally and molecularly the changes that occurs at the myocardium and at the skeletal muscle. Our results showed that we successfully implemented an animal model of HFpEF that presents an LV hypertrophic and increased stiffness. Additionally to LV diastolic dysfunction (DD) we also observed abnormalities on calcium and oxidative stress. In banding rats we denoted an increase of peroxisome proliferator-activated receptor-gamma coactivator alpha (PGC-1α) and downregulation of mitofusin (MNF1,2) as well as an augment of glucose transporters. Despite de increase of uncoupled protein 1 (UCP-1) expression, functionally we denoted an improvement of mitochondria respiration and membrane potential. The physical performance of banding animals was impaired and accomplished by structural changes at skeletal muscle level as well as at metabolic substrate transporters. Curiously, after afterload relief despite the functionally recovery, morphologically the myocardial reverse remodelling was incomplete. Moreover, regardless the metabolic transporters reversion the mitochondria continue smaller. After overload relief the rats showed an improvement on aerobic capacity as well as a reversion on skeletal muscle atrophy, fibrosis and an upregulation of FA oxidation. The present study shows clearly the involvement of mitochondria and metabolism on myocardial and skeletal muscle remodelling and RR.

Abbreviations

ADP: Adenosine diphosphate
AS: Aortic stenosis
ATP: Adenosine triphosphate
A-VO2 dif: Arteriovenous oxygen difference
AVR: Aortic valve replacement
CK: Creatine Kinase
CPT1: Carnitine palmitoyltransferase I
Cr: Creatine
cGMP: Cyclic guanosine monophosphate
CO: Cardiac Output
DD: Diastolic dysfunction
DNA: Deoxyribonucleic acid
ECM: Extracellular matrix
ECO: Echocardiogram
ECT: Electron transport chain
EF: Ejection fraction
eNOS: Endothelial nitric oxide synthase
FA: Fatty acid
FAO: Fatty acid oxidation
GLUT1: Glucose transporter 1
GLUT4: Glucose transporter 4
HF: Heart failure
HFpEF: Heart failure with preserved ejection fraction
HFrEF: Heart failure with reduced ejection fraction
iNOS: Inducible nitric oxide synthase
LV: Left ventricle
LVAD: Left ventricle assist device
LVmass: Left ventricle mass
MMPs: Matrix Metalloproteinases
MFN1: Mitofusin 1
MFN2: Mitofusin 2
mtDNA: Mitochondrial deoxyribonucleic acid
MTPP: Mitochondrial transient permeability pore
NO: Nitric oxide
NPs: Natriuretic peptides
PCr: Phosphocreatine
PDK4: Pyruvate dehydrogenase kinase isoform 4
PGC-1*α*: Peroxisome proliferator-activated receptor-gamma coactivator alpha
PKG: Protein Kinase G
RAAS: Renin–angiotensin–aldosterone system
RCR: Respiratory control ratio
RNS: Reactive nitrogen species
ROS: Reactive oxygen species
RR: Reverse remodelling
SR: Sarcoplasmic reticulum
TGF-β: Transforming growth factor-β
TIMPs: Tissue inhibitors of metalloproteinases
UCPs: Uncoupling proteins
VO_2 max: Maximum rate of oxygen consumption

INDEX

INTRODUCTION

A. General features

The main function of the heart is to provide oxygen and metabolic substrate to all organs and tissues of the body. Heart failure (HF) occurs when the heart cannot pump enough blood to meet the body's metabolic demands, or does it at the expense of high filling pressures [1, 2]. Cardiovascular diseases are the leading cause of death worldwide. In fact, in developed countries, the prevalence of HF is continuously increasing [3]. Despite affecting up to 1-2% of the adult population, its prevalence is expected to increase especially among the oldest and sedentary population [4]. HF results from structural or functional abnormalities in right or left ventricle (LV) that impairs its filling (diastolic dysfunction, DD) or ejection capacity (systolic dysfunction). These alterations can be asymptomatic for a long time before the onset of the first HF manifestations [5]. Despite its clinical relevance, the presence of nonspecific symptoms of HF, hinders its correct diagnosis and treatment [5].

HFpEF is a multifaceted disease with several associated comorbidities and its pathophysiology includes cardiac and extra-cardiac factors [6]. Despite the scarcity of knowledge about HFpEF pathophysiology, it is accepted that it results from a maladaptive process that, despite being initially compensatory to normalize ventricular wall tension, quickly becomes deleterious [7]. Among the pathophysiological mechanism in HFpEF the increase of oxidative stress, abnormal energetic metabolism and dysfunctional mitochondria are currently pointed out as crucial.

Exercise intolerance is a typical signal of HFpEF, very useful to its diagnosis. Moreover, after treatment, some of these patients show improved aerobic capacity. Thus the recognition of skeletal muscle involvement in HFpEF, little is known about its (dys)function or its implication in effort intolerance. Thus, this topic need to be further explored.

The limited knowledge about LV remodelling and RR in HFpEF is reflected on the few therapeutic options available to these patients. Despite the continuous efforts in the discovery of novel therapeutic targets, most of them do not prove efficacy in HFpEF. Moreover, some clinical trials have proved to be ineffective, even harmful, before reaching the phase III [8, 9], and thus, until now these patients remain without an adequate pharmacological therapy.

B. HFpEF definition, epidemiology and diagnosis

HF is classically divided in HF with preserved or reduced ejection fraction (EF), HFpEF or HFrEF, respectively. The most recent guidelines from the European Society of Cardiology

introduced a new subtype for the equivocal cases, when the EF is between 40-49%, named HF with mid-range EF [5]. This HF classification was initially controversial, however the distinct HF pathophysiological mechanisms and therapeutic responses allowed to reach the current consensus [10]. Among all HF cases, those that most concern the medical and scientific community are HFpEF. This syndrome represents more than 50% of all HF cases and is associated to high morbidity and mortality, thus imposing significant costs to the healthcare system, mostly due to high frequency of re-hospitalizations [11].

In HFpEF, LV pressure overload, as arterial hypertension or aortic stenosis, activates several molecular and cellular pathways that triggers LV remodelling through morphological and functional alterations [12]. Over time LV remodelling results in LV hypertrophy and DD, with an augment of LV stiffness, an abnormal filling pattern, an enlargement of the left atrium, pulmonary congestion, etc [6]. At the myocyte level, the cardiomyocytes becomes hypertrophic and stiffer [10]. Although initially thought to be less threatening than HFrEF, a prospective population study observed that HFpEF patients present a survival rate similar to those with reduced EF [13]. Its increased prevalence follow other epidemiologic burdens typical of an sedentary lifestyle such as obesity, hypertension, diabetes and chronic kidney disease [11]. Since HFpEF is also associated with aging and considering the increase of life expectancy, it is presumed that, in 2020, HFpEF will affect more than 8% of the population over 65 years, and will represent nearly 69% of all HF cases. Large epidemiological studies such as the Framingham Heart Study or the Rochester Epidemiology Project showed that HFpEF predominates in elderly female or younger male patients [5, 14, 15].

Additionally to the imperative presence of signs and symptoms characteristic of HF, preserved systolic LV function (LV EF> 50 % and indexed LV end-diastolic volume < 97mL/m²) and evidence of LV DD, the HFpEF diagnosis is also based on plasma biomarkers and imaging methods such as echocardiography [5] or invasive haemodynamic. Regarding DD, pulmonary capillary wedge pressure (PCWP)> 15mmHg, LVEDP> 12mmHg at rest or E/e'>15 provide sufficient evidence of DD. When E/e' is in the range of 8–15 or NT-pro natriuretic peptide type B (BNP)/BNP levels are higher (NT-proBNP>220pg/mL; or BNP> 200pg/mL) is necessary at least one additional sign of DD, including a low E/A ratio combined with a high deceleration time, pulmonary venous flow patterns indicative of DD, increase left atrium, atrial fibrillation, and/or LV hypertrophy [16]. Additionally to the routinely use of BNP as a biomarker, other molecules such as procollagen, inflammatory factors such as interleukin-6 and -8, thyroid hormones, troponin T, proteins involved in the transport of fatty acids (FA), carbohydrate *antigen* 125 (*CA125*) are also used in HFpEF, however, they still await validation [17]. In the ambiguous cases, the effort intolerance test determined by echocardiography is performed through a diastolic stress test and using a dynamic exercise protocol [5].

C. Metabolic myocardial changes and implications for cardiac function in HFpEF

Compared to other cells of the organism, cardiac myocytes are those who consume more energy. ATP is mainly produced by mitochondrial oxidative phosphorylation and regulated by an efficient system of energy transfer. The concept that cardiac muscle is energetic starved was introduced in 1939 by Dechered [18] and demonstrated posteriorly by several authors. Actually, all the processes involved in production/extraction, transfer or utilization of energy are reduced in HF, which compromise the function and integrity of cardiac muscle (35). The process of ATP regeneration is centred in a reaction catalysed by creatine kinase enzyme (CK), that transfer a phosphate group from phosphocreatine (PCr) to ADP. This reaction allows not only to regenerate ATP and creatine (Cr) but also to prevent ADP accumulation.

In an adult heart, approximately 70% to 90% of cardiac ATP is produced by the oxidation of FAs [19]. However, heart is an organ extremely flexible, capable of generating energy from oxidation of other substrates, such as carbohydrates (lactate, glucose), ketones and amino acids [20]. This cardiomyocyte plasticity is essential for the myocardium to meet its high metabolic demands and to quickly adapt to the constant hemodynamic and/or metabolic changes [21]. Therefore, energetic pathways such as oxidative phosphorylation, citric acid cycle and FA oxidation are essential for maintaining a normal contractile function. Several authors have reported this myocardial metabolic flexibility, especially under pathologic conditions, such as in the hypertrophic heart, where a metabolic substrate shift is observed [22-26]. Unlike physiological hypertrophy, where an increase of FA and glucose oxidation is observed, pathological hypertrophy is characterized by a shift towards glucose utilization [22, 23, 26] accompanied by a downregulation of genes involved in FA metabolism [27]. Despite the relative consensus regarding the reduction of FA oxidation in the hypertrophic myocardium, some studies describe the increase of glycolysis accomplished by a decrease or unchanged FA oxidation [22-24]. These inconsistencies could probably be explained by the degree of hypertrophy, severity of HF and its impact on cardiac metabolic profile, as well as by the differences on the animal model. The underlying mechanisms that trigger decreased FA oxidation remain unknown, however, changes in the expression of genes involved in FA metabolism (like activation gene for FA (GOA) and PPAR-α) [22, 26], abnormal FA absorption (despite normal CD36 expression) [22] or a carnitine deficiency [23] seems to be involved. The heart can fine-tune ATP consumption to its energetic needs [28], but the net yield of ATP production per mole of FA oxidation is greater than per mole of glucose, despite lower oxygen costs for the latter. So, this metabolic shift toward glucose compromises the energetic state of the myocardium [20].

In the hypertrophic heart the metabolic modifications are not restricted to oxidative substrate, since the uncoupling between glycolysis rate and glucose oxidation is also reported and seems to contribute to heart dysfunction and its subsequent progression to HF [7, 23, 29]. Nevertheless, it is clear that myocardial remodelling is associated to metabolic alterations, which in turn are accompanied by alterations in enzymes that regulate carbohydrates and FA metabolism. Recently it was suggested that the alterations on metabolic substrate that occurs in myocardium impact contractile dysfunction and contributes to progressive HFpEF myocardial remodelling [30]. Hence, optimization of the energy production or the metabolic substrate could represent a potential therapeutic target for HFpEF.

i. Energetic deficit in HFpEF

Many of the comorbidities associated to DD and HFpEF are related to cardiac metabolic perturbations capable of modifying the amount of adenine and creatine compounds, and thus affecting myocardial function [31]. Actually, a linear relationship has been described between ATP hydrolysis, actin-myosin interaction and contractile force [3, 32-34] as well as between ADP levels and tele-diastolic pressures [35].

In HFpEF, the evidence of a deficient energetic reserve is confirmed by the reduction of the PCr/ATP ratio that can be ascribed to PCr decrease [36] or, in some cases, to a drop of 30-40% in ATP levels in failing hearts. In pathological hypertrophy, the increase of glycolysis activity [27] culminates in a decrease of mitochondrial oxidative metabolism and thus a reduction in the content of ATP, Cr and PCr [37, 38]. In fact, the reduction of PCr levels results in a deficit of conversion of ADP to ATP and impairs the ratio ATP/ADP [35]. Moreover, elevated levels of ADP augment the filaments sensitivity to Ca^{2+} and increase the recruitment of cross-bridges, culminating in a slower myocardial relaxation [36, 39, 40] and greater cardiomyocytes stiffness [39]. Moreover, in rats, the reduction of the contractile reserve, the increase of LV end-diastolic pressure and mortality was associated to PCr reduction or a CK inhibition [35].

In the myocardium, free energy resulting from ATP hydrolysis is used for several mechanisms, being 60-70% directed to contraction and relaxation and the remaining 30-40% used by sarcoplasmic reticulum (SR) Ca^{2+}-ATPase (SERCA-2a) and by others ion pumps [3, 41]. A relevant fact for HFpEF is the finding that the diastolic consumption of ATP exceeds the one of systole [41]. Indeed, during relaxation, ATP hydrolysis is necessary to release ADP from myosin heads and decouple myosin heads form actin filaments, dissociating Ca^{2+} from troponin C and to reuptake Ca^{2+} to SR. Thus, additionally to ATP, calcium is also crucial to myocardial relaxation by

regulating ATP synthesis and consumption during cardiac cycle [41, 42]. Therefore, an abnormal relaxation associated to DD, as occurs in HFpEF, can also result from alterations in filaments sensitivity to Ca^{2+} and diastolic reuptake of Ca^{2+} [43]. Indeed, the rate at which SERCA-2a pumps Ca^{2+} to SR during diastole is ATP-dependent, so changes in SERCA-2a activity can also be associated to the reduction of ATP content [44]. In HFpEF, alterations on Ca^{2+}reuptake could result from the reduction on SERCA-2a activity or an increase in the phosphorylation of phospholamban (a SERCA-2a inhibitor). Both can change myocardial Ca^{2+} kinetics and ventricular relaxation [41, 45, 46]. Additionally, hyperphosphorylation of ryanodine receptors can also underlie the reduction of the content of Ca^{2+} in SR and therefore contribute to increase Ca^{2+} cytosolic and the worsening of myocardium relaxation [31, 44]. It becomes evident that a normal diastole depends on the proper function of metabolic processes capable of regenerating ATP. Thus, low energy reserve observed in HFpEF can result from mitochondrial dysfunction or metabolic substrate alteration. However it is not known whether these alterations are a cause or consequence of HF [3].

D. Mitochondrial alterations in HFpEF

One cannot describe alterations in energetic metabolism in HFpEF without referring to mitochondria, considered the "key-organelle" of the cell energetic machinery. The relationship between mitochondrial dysfunction and HF was suggested in 1962, when Schwartz & Lee observed a reduction in mitochondrial oxidative phosphorylation capacity in pigs that developed HF after aortic constriction [47]. Cardiomyocyte's impressive content in mitochondria (>30% of its total volume) reflects the importance of oxidative phosphorylation for this organ. In fact, on adult individuals, under normoxia and resting conditions, about 95% of the myocardial ATP demands comes from mitochondria [3, 19]. Structural and functional alterations of mitochondria have been described in several cardiovascular diseases, namely HF. The proposed mechanisms for mitochondrial dysfunction are diverse and include: i) electron transport chain dysfunction; ii) modifications in mitochondrial complexes organization; iii) increased oxidative stress; iv) alteration of membrane lipid profile with decreased cardiolipin content; v) changes in the Krebs cycle and vi) mitochondrial uncoupling [48].

The reduction of energetic reserve and the abnormal relaxation observed in HFpEF could involve mitochondrial dysfunction. This hot topic has recently attracted attention of many researchers, since there are several evidences that these alterations are the cause of metabolic remodelling, energy deficiency and increased oxidative stress (**Figure 1**).

i. Oxidative phosphorylation, biogenesis and mitochondrial coupling

Mitochondrial energy production involves the coupling between electron transfer and oxygen uptake through the electron transport chain complexes (CI, CII, CIII, and CIV) and the phosphorylation of ADP (CV) [49]. The dysfunction of this process, evidenced by the decrease of mitochondrial respiration rate and consequent decrease of ATP content, is consistently observed in the HF [50]. In HF patients changes in complex I of the electron transport chain have been reported [17], while in rats, complexes III and IV were also shown to be dysfunctional [51]. In compensated hypertrophy the increase in mitochondrial respiration is sustained until systolic dysfunction begins, declining thereafter [19, 52]. These observations raise the question if the dysfunction in mitochondrial oxidative phosphorylation is responsible for the HF progression.

The involvement of mitochondrial biogenesis in compensated hypertrophy and DD is controversial since changes in the expression of biogenesis proteins, like PGC-1alpha, ERRalpha and Tfam, are inconsistent [30, 44]. In humans with compensated hypertrophic cardiomyopathy a decrease of mtDNA content was associated to downregulation of mitochondrial biogenesis and decreased expression of proteins involved in mtDNA maintenance [53]. However, other authors described an overexpression of proteins involved in biogenesis. These authors state that the downregulation of proteins involved in biogenesis could be related to mitochondrial damage and mitophagy activation [54], and thus represent a mechanisms triggered by mitochondrial loss and injury. In dogs with aortic coarctation-induced hypertrophy, mitochondrial ultrastructure was normal. Moreover, mitochondria, isolated from epicardial and endocardial regions of these hypertrophic hearts showed normal rates of respiration, ATP phosphorylation, citrate synthase, and cytochrome c oxidase activity compared to control dogs [55].

When oxidative phosphorylation occurs independently of ATP production the mitochondria are uncoupled. Mitochondrial uncoupling may be caused by intrinsic issues of respiratory chain proteins, but may also be a consequence of increased expression or activity of uncoupling proteins (UCPs). The UCPs are located in the inner mitochondrial membrane, and their function is to dissipate the electrochemical gradient, diverting the electron flow from ATP synthesis and subsequently increase heat production. The main purpose of UCPs is to regulate energetic metabolism and mitochondrial reactive oxygen species (ROS) production, however, they also decrease the ADP/O ratio affecting the oxidative phosphorylation efficiency [13, 56]. Changes in the expressions of UCP2 and UCP3 have been found in several types of HF [27, 57] and LV hypertrophy [22, 24]. An animal model of HF secondary to aortic regurgitation showed that the LV expression of UCP2 differs according to HF progression, being decreased at early stage and overexpressed at the final stage of HF. Interestingly, in the end-stage of HF, a concomitant increase

of TNF-α and a decrease of PCr content was also observed. Given these results, the authors suggested that TNF-α could be involved in the upregulation of UCP2, which, in turn, would be responsible for PCr decrease and, therefore, implied in the lower cardiac energy efficiency observed in HF [27]. Regarding the mitochondrial alterations and UCPs, their role in the HF pathophysiology has not been completely elucidated. It is unknown if this is an adaptive phenomenon that aims to reduce oxidative stress, or a deleterious phenomenon, being involved in mitochondrial energetic dysregulation (**Figure 1**).

E. Reactive Oxygen Species

In mitochondria, ROS production usually occurs during a normal mitochondrial metabolism. The problem arises when the increased levels of ROS are not balanced by antioxidant systems and becomes pathological, as recently described for HFpEF [41]. In mitochondria, the pathological increase of ROS is mainly a consequence of the incomplete reduction of oxygen that occurs in complexes I and III [41]. In mice hearts, who developed HFpEF after chronic pressure overload or administration of angiotensin II, an increase in mitochondrial ROS with consequent dysfunction of the organelle (decreased membrane potential, increased protein oxidation, as well as deletions in mitochondrial DNA (mtDNA)) and activation of the MAPK pathways has been described [54]. Similar results were obtained from another group that assumed that elevated oxidative stress would underlie mitochondrial damage and cardiac dysfunction [51]. Effectively, ROS upregulation can lead to extensive oxidative damages in a variety of molecules, such as proteins, DNA and lipids. Moreover, ROS can also modulate several signalling pathways involved in ventricular hypertrophy progression, contractile dysfunction, Ca^{2+} deregulation and myocardium stiffness, leading to increased passive tension of cardiomyocytes [29, 41, 49]. It was also reported that in the hypertrophic and stiffened myocardium, the primary source of ROS is the mitochondria. In fact, treatment with mitochondrial antioxidants improved angiotensin II-induced cardiomyopathy [54].

I. ROS and nitric oxide

In the presence of ROS, nitric oxide (NO) and nitric oxide synthase (NOS) are oxidized, decreasing NO bioavailability [58] and consequently its beneficial effects including the control of mitochondrial pore opening [59]. Haemoglobin and myoglobin regulate NO, a potent vasodilator, and oxygen (O_2) gradients in myocardium, removing NO when O_2 concentrations are high and providing it when O_2 concentrations decrease in order to properly adjust blood flow to the tissue metabolic needs [59]. In the presence of low O_2 concentrations, NO binds reversibly to O_2 binding site on cytochrome c oxidase, adjusting the mitochondrial O_2 consumption to the tissue content. In HF, the dysregulation of this mechanism is associated to impaired myocardial O_2 consumption (MVO_2) and the progression of compensated to decompensated HF [60]. High amounts of NO or its derivatives, reactive nitrogen species (RNS), regulate oxidative phosphorylation by inhibiting mitochondrial respiration by two distinct mechanisms, NO inhibition of cytochrome c oxidase, in an acute, powerful and reversible manner through competition with O_2 or by irreversible and generalized inhibition by RNS [61]. The latter occurs because RNS induces post-translational modifications in these proteins, such as nitrosylation or oxidation of thiol groups and removal of iron from ion-sulfur centers [62]. As a consequence, the production of ATP decreases while ROS and RNS increases, causing significant changes in myocardial intracellular signalling pathways and contributing to cell death [59]. In rats who developed hypertrophy by aortic constriction there was a concomitant increase in NO sensitivity in complex IV of the respiratory chain and in the production of inducible nitric oxide synthase (iNOS) [63]. High levels of ROS also increase the activity of the protein phosphatase 2a, that decrease the phospholamban phosphorylation and consequently diminish SERCA-2a activity, resulting in a decrease of Ca^{2+} reuptake by the RS [64]. Additionally, post-translational modifications induced by ROS and RNS can cause alterations in Krebs cycle enzymes (eg. aconitase) or inhibit proteins such as CK [59]. NO can also interfere with mitochondrial biogenesis via cGMP or by enhancing the stimulation of transcription factors, such as PGC-1alpha, NRF-1 or mtTFA, resulting in increased expression of respiratory chain complexes [59].

In HFpEF, reduced NO bioavailability can be due to this imbalance between ROS and NO, which results in impaired activation of myocardial cGMP-PKG. Moreover, treatment with BH4, a cofactor of NO synthesis, improved diastolic dysfunction [43] and activation of NO-cGMP-PKG pathway reduced the sensitivity of the myofilaments to Ca^{2+} [65, 66]. The downregulation of NO-cGMP-PKG pathway is also associated to deleterious structural (hypertrophic remodelling with increased fibrosis and cardiomyocyte hypertrophy) and functional (systolic and diastolic dysfunction) effects [15, 67]. In HFpEF, decreased activity of PKG reduces titin phosphorylation

and increase myocardial stiffness [68]. Additionally to phosphorylation degree, titin post-translational modifications induced by oxidative alterations are important modulators of cardiomyocyte passive strength that can decrease its distensibility and thus contribute to increased passive tension [69].

Besides NOS uncoupling, decreased NO bioavailability can result from endothelial dysfunction [70]. Overproduction of ROS/RNS from endothelial cells and decreased NO bioavailability in the myocardium have recently been shown to be important determinants of myocardial disease progression in both hypertensive and HFpEF patients [15, 70].

II. ROS and ECM

Endothelial dysfunction and oxidative stress seems to be important mediators of inflammation, which are present in both HF subtypes [71]. In aortic valve disease, the rise of inflammatory mediators in endothelial cells increases oxidative stress, triggering the activation of the osteogenic and fibrogenic pathways, promoting valve calcification, and thus increased LV afterload [72]. In the 1990s, inflammation and fibrosis were shown to increase with LV hypertrophy. More recently, oxidative stress was proposed to trigger TGF-β activation thus increasing collagen synthesis and inhibiting its degradation [73, 74]. Collagen is a crucial element of the extracellular matrix (ECM), essential to maintain the structural composition of the myocardium, to assist mechanotransduction and, together with other proteins such as elastin, to contribute to the elastic properties of the heart [45]. In HFpEF, ECM alterations result from changes in collagen metabolism, mainly in type I and type III collagen, which are the most abundant in cardiac tissue (>90%). These changes include alterations in their deposition, degree of cross-bridging and relative amount, resulting in the development of myocardial interstitial fibrosis and subsequent ECM stiffening [75]. The activation of myofibroblasts, which are responsible for the fibrotic tissue remodelling, is due to the activation of several proteins and hormones, such as the renin-angiotensin-aldosterone system (RAAS) [76], a crucial neurohumoral axis in HFpEF [10]. Collagen metabolism results from the balance between metalloproteinases activity (MMPs) and their tissue inhibitors, TIMPs, as well as other proteins. In hypertensive patients with HFpEF, a downregulation of MMPs and an overexpresion of TIMPs [77] have been described, resulting in a decrease in ECM degradation that contributes to increased ventricular stiffness (**Figure 1**) [46].

In HFpEF patients, the presence of cells with an inflammatory profile leads to the release of factors, such as TGF-β, responsible for inducing production of collagen and differentiation of fibroblasts into myofibroblasts. TGF-β by producing cytokines and chemokines stimulates the

recruitment and activation of more inflammatory cells. This inflammatory profile seems to arise early in the progression of cardiac pathology. Indeed, MCP-1 protein and TGF-β increase in compensatory hypertrophy and molecules such as interleukins (IL-6, IL-18 e IL-17R), TNF-α, anaphylatoxin C5a or ST-2 appear to be involved in DD progression. Markers of fibrosis and systemic inflammation such as galectin-3 and growth differentiating factor 15 (GDF15) arise as promising indicators of HFpEF progression [46].

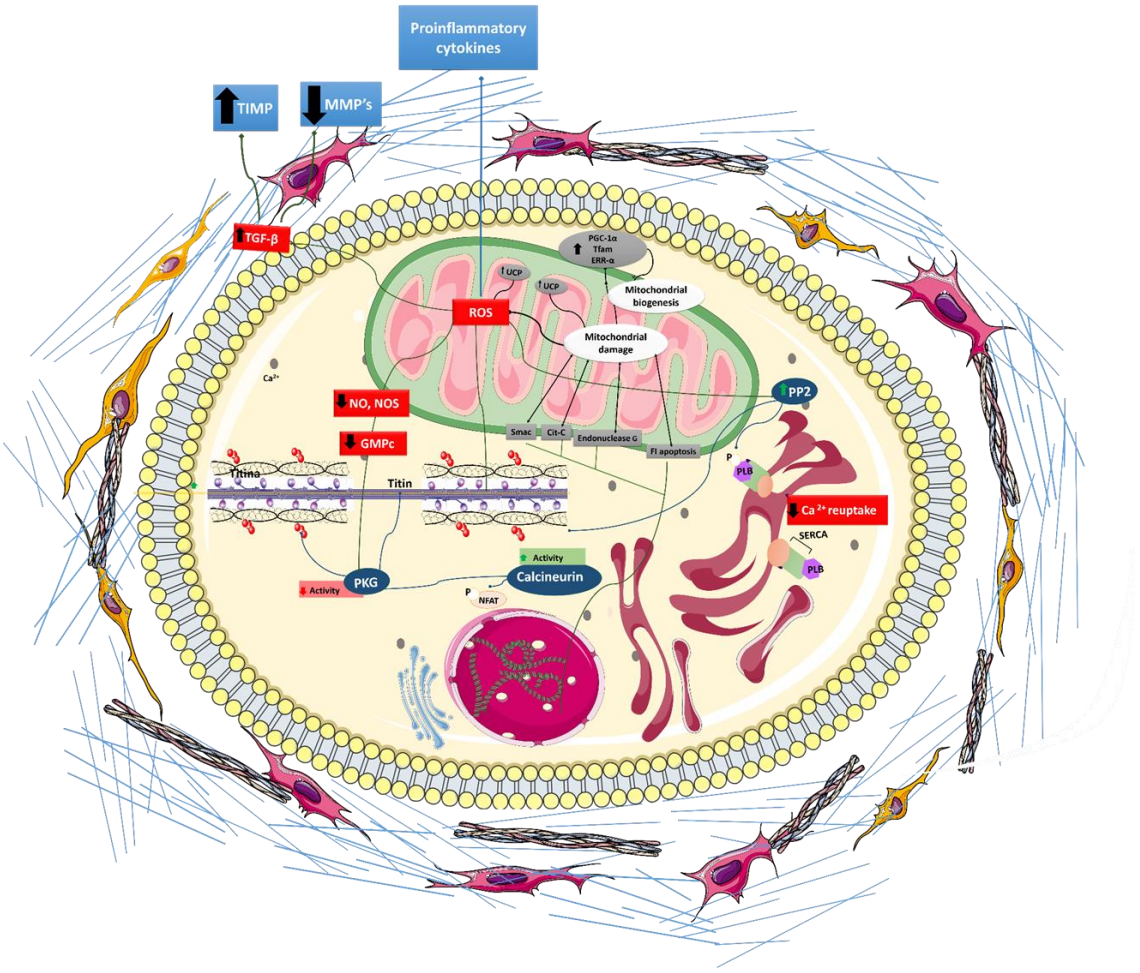

Figure 1: Alteration of energetic substrate and mitochondrial dysfunction on the basis of functional changes of the hypertrophic myocardium. The energetic dysfunction of the myocardium, underlying the change of oxidative substrate leads to mitochondrial dysfunction. Mitochondrial dysfunction culminates in increased ROS, which, by decreasing NO and NOS bioavailability reduce PKG and phosphorylation of titin. Increased ROS–mediated protein phosphatase 2 (PP2) activity inhibits phospholamban phosphorylation and decreases SERCA-2a activity, thereby altering relaxation. ROS act directly on titin, increasing its passive tension. Mitochondrial proteins released from the intermembrane space (Smac, cytochrome C, apoptosis inducing factor, etc) leads to DNA fragmentation and triggers apoptotic events. ROS may also contribute to extracellular matrix stiffness by promoting matrix remodelling and proinflammatory cytokines. PLB, phospholamban; NO, nitric oxide; NOS, nitric oxide synthase; TGF-β, transforming growth factor beta; ROS, reactive oxygen species; cGMP, cyclic guanosine monophosphate; MMPs, matrix metalloproteinases; TIMP, tissue inhibitors of matrix metalloproteinases; PP2, protein phosphatase 2a; PKG, cGMP-dependent protein kinase.

F. Exercise intolerance in HFpEF

In addition to HFpEF-induced metabolic, structural and functional alterations in cardiac muscle, HFpEF also promote relevant consequences at the skeletal muscle level. The close relationship between these two muscles is probably due to the high metabolic requirements of the skeletal muscle during exercise as well as the similarities among both organs. Therefore, in some cases, skeletal muscle abnormalities could be an indicator of myocardium performance [37].

Exercise intolerance is a common hallmark among HFpEF patients that often arises as an early symptom of the disease. The aerobic capacity, usually evaluated by the peak of oxygen uptake (VO_2) is an important determinant of quality of life and mortality in HFpEF and is reduced ~40% of these patients [78, 79]. Contrary to HFrEF, in HFpEF the mechanisms that underlying low aerobic capacity are poorly explored [80]. According to Fick equation, peak VO_2 corresponds to the product between cardiac output (CO) and the difference in the arterial-venous oxygen content (A-VO_2 diff). During exercise the needs of O_2 rise, therefore an increase of CO, A-VO_2 diff or both is required. Thus, a reduced peak VO_2 during exercise may be the result of decreased CO and/or reduced utilization or delivery of O_2 to muscles [80]. Furthermore, alterations on heart rate induced by exercise correlates more to peak VO_2 than to stroke volume [78].

When subjected to physical exercise, HFpEF patients show an incapacity to increases CO adequately [81]. The compromised CO is associated to chronotropic incompetence [82], inadequate systolic reserve [83] and ventricular-vascular coupling [84]. Other changes, such as capillary rarefaction [85], endothelial dysfunction [83] and abnormal vasodilatation [82] were also reported as underlying exercise intolerance in HFpEF patients. Among cardiac alterations, the inadequate CO reserve together with elevated filling pressures are pointed out as the main reason for exercise intolerance [86].

In addition to the contribution of cardiac alterations to exercise intolerance in HFpEF, it has been proposed that, an inadequate oxygen extraction and/or utilization as well as skeletal muscle alterations may also play a major role. Thus, non-cardiac factors, such as skeletal muscle dysfunction [79, 87] could be involved in reduced aerobic capacity. To support this idea there are some studies showing that, the abnormal response to maximal and submaximal exercise in HFpEF patients was not due to alterations in hemodynamic and cardiac reserve parameters, but to irregularities in extraction and/or utilization of O_2 (A-VO_2 diff), increased peak CVO_2 (oxygen content in venous blood) as well as intrinsic abnormalities in skeletal muscle [79, 81]. Moreover, it is noteworthy that in HFpEF patients the increase of VO_2 at exercise peak was due to an augment of A-VO_2 diff, despite the absence of correlation between CO and A-VO_2 diff [82]. In v*astus lateralis* muscle biopsies from HFpEF patients, the reduction in the capillary/fibre ratio and the

decrease of type I oxidative fibres, correlated both positively to peak VO_2 and 6-min walk distance [87]. Moreover, diaphragm muscle from HFpEF rats show a different pattern of fibre type shift, from fast glycolytic fibres (type II) to slow oxidative fibres (type I), and atrophy of both muscle fibres types [88]. Together, these alterations may be at the origin of limited oxygen diffusion, decreased of mitochondrial density and its reduced oxidative capacity, observed in skeletal muscle biopsies from HFpEF patients. Moreover, these biopsies have a 54% reduction of mitofusin 2 expression, which clearly evidence changes in mitochondrial biogenesis and mitochondria-SR coupling. Importantly, both porin and mitofusin 2 expression correlates positively with peak VO_2 and 6-min walk distance [89], which denote the functional implications of these findings. A reduction of proteasome activity and mitochondrial alterations at complex I level with decreased oxygen consumption and decreased respiratory control ratio (RCR) have been reported in mitochondria from skeletal muscle [88]. In addition, changes in muscle redox balance were detected, with an increase of antioxidant proteins (catalase) and reduction of pro-oxidant proteins (NADPH and xanthine oxidase), indicating an attempt to reduce oxidative stress [88].

G. Reverse Remodelling

The heart is an organ with a high capacity to adapt to the deleterious stimuli. When these stimuli cease or attenuate, the myocardium undergoes a process called reverse remodelling (RR), which usually results in an improvement of its structure and function. RR can be defined by any myocardial changes that can be reversed chronically through pharmacological or surgical treatment [90]. If the knowledge on myocardial remodelling in HFpEF is scarce, the available information regarding RR is even more limited and derives mainly from patients with aortic stenosis (AS) with DD that undergo RR after aortic valve replacement (AVR). Despite the lack of literature regarding the molecular and cellular mechanisms underlying RR in HFpEF, it has been described some functional and structural alterations on LV, such as regression of cardiac hypertrophy, normalization of tele-systolic and tele-diastolic volumes, as well as an improvement in the filling pattern [68]. Moreover the myocardial response of the patients after valve replacement can diverge, ranging from a total improvement to partial recovery of cardiac function, being the latter an indicator of poor prognosis [20]. Actually, early after AVR some AS patients showed an augment of LV stiffness, which was associated to increase of interstitial fibrosis that occurs independently of LV mass reduction. Later after AVR, myocardial stiffness decreases in parallel with the decrease in hypertrophy and fibrosis, albeit remaining higher than control subjects [91]. The regression of LV hypertrophy is often incomplete and occurs later, matching the improvement of LV performance.

Indeed, 6 months after AVR, the mass regression does not exceed 31% [31, 92]. HFpEF hearts are often hypertrophic and since LV mass regression results in a reduction of clinical events [71], the patients that show higher LV mass after AVR still represent a risk group to cardiovascular events. Villari *et al*., showed that the improvement on myocardial perfusion appears to be an important adjuvant in LV RR [76]. In a recently published retrospective study involving severe AS patients who underwent AVR, the baseline diastolic dysfunction score remained the most important echocardiographic factor associated with adverse 1-year outcomes, despite the improvement on diastolic function after surgery [93]. It is important to note that these clinical studies were made in patients with HF that underwent AVR and not in pure HFpEF patients. In rats, after ventricular unloading, it has recently been described a regression on LV mass, cardiomyocytes hypertrophy and fibrosis and an improvement of ventricular-arterial coupling and energy efficiency [94]. Recently, in a rat model of hypertension-induced HFpEF treated with cardiosphere-derived cells with anti-fibrotic and anti-inflammatory properties, the functional abnormalities of HFpEF were suppressed and survival rate was improved, while either blood pressure or cardiac hypertrophy remained unchanged [95].

Concerning the molecular and cellular changes that occur during LV RR, the available knowledge derives mainly from HFrEF patients, in whom the eminent cardiac failure is delayed by the implantation of a LV assist device (LVAD). These devices support cardiac contractile function, representing a bridge for cardiac transplantation. Parameters such as EF, cardiac chambers dimensions and LV wall thickness are used as predictors of myocardial recovery after LVAD. In fact, the patients whose EF increases above 50% have a better prognosis after removal of the device [49]. As reported by Mital *et al*., the beneficial effect of LVAD occurs early after its implantation with a significant increase of endogenous NO, a reversal of mitochondrial uncoupling and an improvement of myocardial oxygen consumption (MVO_2). Curiously, these beneficial effects were attenuated by NOS inhibition [49]. After removal of the LVAD the myocardium improves significantly and, apart the reduction of fibrosis and cardiomyocyte hypertrophy [45], a clear improvement of Ca^{2+} kinetics was observed (increased Ca^{2+} reuptake to RS, faster inactivation of type L Ca^{2+} channels and increased Na^{+}/Ca^{2+} channels expression) [45]. Furthermore, the improvement of myocardial performance was followed by the upregulation of enzymes involved on Krebs cycle and on pyruvate metabolism, thus improving glucose and FA oxidation [96]. Such is the case of arginine glycine amidinotransferase, an enzyme involved in creatinine synthesis, whose levels normalize in patients displaying a good pattern of RR [45]. Despite the importance of energetic and mitochondrial metabolism for RR, surprisingly, not many studies have focused on this topic. Recently, Lee and others have reported that mitochondrial respiration, which is severely compromised in patients with advanced HF, improves significantly

after LVAD implementation [97] Moreover, an improvement of coupling between oxidative phosphorylation and electron transport, a decrease of ROS (through decrease of premature reduction of O_2 to O_2^- and, a better energy efficiency and myocardial performance was observed in these in these patients [49]. The improved mitochondrial performance after LVAD can be caused by the increase of cardiolipin content [29, 49, 98]. Conversely, increased oxidative stress and DNA damage are also reported after LVAD [99] but these findings are more frequent in patients with systemic inflammatory response syndrome [100].

In a mouse model of TAC-induced HF, mitochondrial dysfunction and oxidative phosphorylation were significantly affected. Most of the mitochondrial and metabolic-related proteins were downregulated in parallel with the decline in mitochondrial DNA copy number. After SS-31 peptide treatment the improvement of myocardial performance occurs in parallel to attenuation of mitochondrial damage suggesting that perturbed mitochondrial function may be an upstream signal to many of the pathway alterations in TAC [8]. It is currently recognize that myocardial dysfunction in patients with advanced HF could be, at least in part, reversible and mitochondria seems to be compromise in RR. However if mitochondria have a similar role in HFpEF RR still unknown [49].

After LVAD implementation, exercise capacity was improved [101], and the patients showed a better aerobic capacity. However, if cardiac muscle, skeletal muscle or both are behind this improvement remains unknown. Currently the clinical trial “Skeletal Muscle Perfusion With LVAD” is ongoing and aims to evaluate the skeletal muscle perfusion after RR.

AIMS

The aims of this work are to:

1. Implement and characterize an animal model of myocardial remodelling and reverse remodelling associated to HFpEF
2. Evaluate the myocardial alterations associated to:
    a. Cardiomyocyte and extracellular matrix remodelling
    b. Calcium handling
    c. Oxidative stress
3. Characterize the cardiac metabolism, including mitochondria structure and function
4. Assess the changes in skeletal muscle, namely in terms of:
    a. Exercise capacity
    b. Skeletal myocyte and matrix remodelling
    c. Skeletal muscle metabolism

METHODS

1. Experimental animal model

I. *Ascending Aortic Banding and Debanding*

Young male Wistar rats (±50g) were anaesthetized by inhalation of 8% sevoflurane in vented containers, orotracheally intubated and mechanically ventilated (TOPO Small Animal Ventilator, Kent Scientific Inc). Anaesthesia was maintained with sevoflurane (1-2.5%). Rats were placed in right-lateral decubitus on a heating pad, ECG was used to monitor heart rate and temperature was kept at 38ºC. The skin was shaved and disinfected with iodopovidone solution. Aortic banding was done surgically through a small incision performed between the 2nd and 3rd intercostal space to access and dissect the ascending aorta. A suture was placed around the aorta and quickly tight against a 22 gauge blunt needle (Banding group, Ba). In the sham group, the suture was kept loose (Sh group). After 8-9 weeks, a second surgery was made in half of the banding animals to remove the suture. These animals gave rise to an additional group – debanding group (Deb) (**Figure 2**). Experiments were performed according to the Portuguese law for animal welfare and to the Guide for the Care and Use of Laboratory Animals published by the National Institutes of Health (NIH Publication 85-23, Revised 2011).

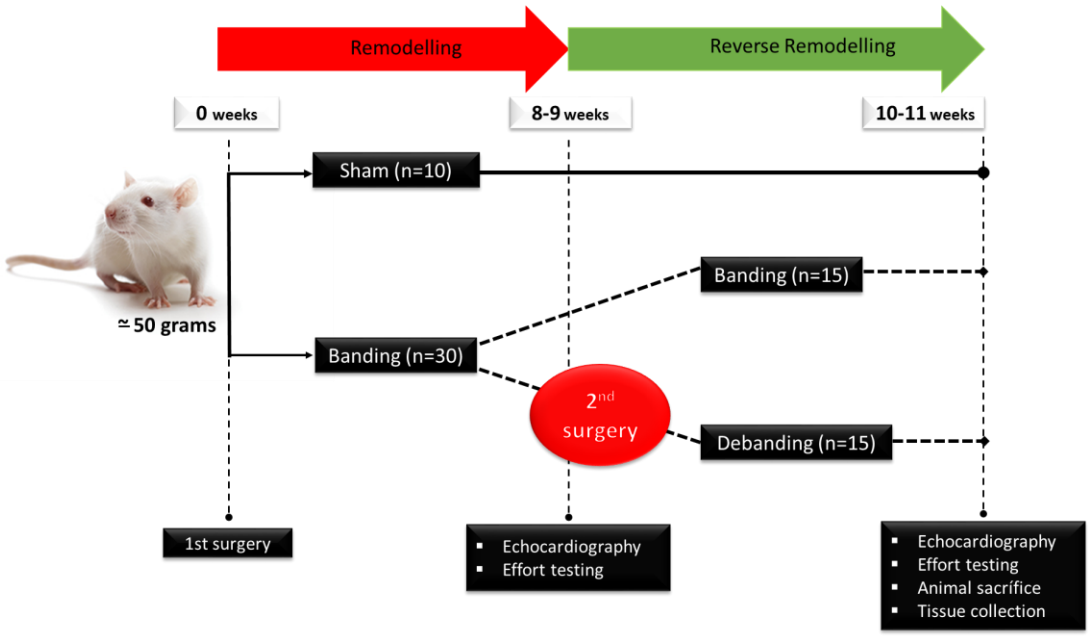

Figure 2- Design of experimental groups.

2. Echocardiographic evaluation

All the experimental groups of rats (Sh=10, Ba=15, Deb=10) were anaesthetized by inhalation of 8% sevoflurane in vented containers, orotracheally intubated and mechanically ventilated (TOPO Small Animal Ventilator, Kent Scientific Inc). Anaesthesia was maintained with sevoflurane (1-2.5%) and titrated to avoid the toe pinch reflex. Rats were placed in left-lateral decubitus on a heating pad, the ECG was monitored and their temperature was kept at 38ºC. The skin was shaved and disinfected. After applying prewarmed echocardiography gel a linear 15MHz probe (Sequoia 15L8W) was gently positioned on the thorax. Systolic and diastolic wall thickness and cavity dimensions were recorded to assess M-mode at the level just above the papillary muscles in the parasternal short axis view. To assess EF, fractional shortening (FS), end diastolic (EDV) and end systolic volumes (ESV) and to calculate LV. The EF and FS were calculated using the formulas $LVEDD^2$-$LVESD^2$)/$LVEDD^2$ and (LVEDD-LVESD)/LVEDDx100, respectively. LV mass was estimated using the formula previously validated in small animals and adjusted for body weight: [LV-mass= $\{(SWT+PWT+LVEDD)^3-(LVEDD)^3\}\times 1.05$]. Transverse aortic root diameter was recorded by M-mode echocardiography, in the parasternal long axis view. Aortic flow velocity was assessed by pulsed-wave Doppler just above the aortic valve. stroke volume (SV) was calculated by aortic flow as the product of the aortic area and the velocity time integral (VTI) of the pulsed wave Doppler (VTI). Cardiac output was calculated as the product of SV and heart rate (HR). Mitral flow velocity tracings were obtained with pulsed-wave Doppler just above the mitral leaflets, peak systolic tissue velocity and E' were measured with tissue Doppler at the medial and lateral mitral annulus and lateral mitral annulus, respectively, and left atrial dimensions were measured, at their maximum, by 2D echocardiography in the four chamber view. Acquisitions were done using an echocardiograph (Siemens Acuson Sequoia C512) while transiently suspending mechanical ventilation. Recordings were averaged from three consecutive heartbeats

3. Aerobic capacity and effort testing

To determine the maximum oxygen consumption (VO_2max), by maximum effort test, all experimental groups of rats were placed on a treadmill camera coupled to a gas analyzer (LE8700C and LE405, Panlab Harvard Apparatus ®). The gas flow was set at 700 mL/min and the treadmill inclined at 10°. The adaptation period were carried out at a speed of 15 $cm.s^{-1}$ for 3 minutes. The protocol was performed at a speed of 30 $cm.s^{-1}$, with increments of 5 $cm.s^{-1}$ every minute until the animals reached its maximal aerobic capacity.

4. Animal sacrifice and sample collection

All the experimental groups of rats (Sh=10, Ba=15, Deb=10) were anaesthetized by inhalation of 8% sevoflurane in vented containers, orotracheally intubated and mechanically ventilated (TOPO Small Animal Ventilator, Kent Scientific Inc). Anaesthesia was maintained with sevoflurane (1- 2.5%) and titrated to avoid the toe pinch reflex. Subsequently the animals were sacrificed and the tissues collected for molecular and functional studies.

5. Mitochondrial studies

I. Isolation of heart mitochondria

Cardiac mitochondria were freshly isolated using differential centrifugation methods. The heart was harvested and minced in an ice-cold isolation buffer containing 250 mM sucrose, 10 mM Hepes, 1 mM EGTA, pH 7.4 and 0.1% defatted BSA. Minced blood-free tissue was then mechanically homogenized with a glass Potter-Elvejhem in the presence of isolation medium (7 g/50 mL). The homogenate was centrifuged at 800×g for 10 min at 4°C and the resulting supernatant was centrifuged at 10,000×g for 10 min at 4°C. Mitochondrial pellet was resuspended and centrifuged twice at 10,000×g for 10 min to obtain a final mitochondrial suspension. Both EGTA and BSA were omitted from the medium (250 mM sucrose, 10 mM Hepes pH 7.4) in the two last centrifugations. After isolation, mitochondrial protein was determined by the Biuret method [102] using BSA as standard. Aliquots of heart mitochondrial suspension were separated and frozen at −80°C for later analysis. The remaining fresh isolated mitochondria fraction was used within 3–4 h after the excision of the heart and were kept on ice (0–4°C) throughout this period.

II. Mitochondrial oxygen consumption assays

Oxygen consumption of isolated mitochondria was determined polarographically at 25°C with a Biological Oxygen Monitor System (Hansatech Instruments) and a Clark-Type oxygen electrode (Model DW1, Hansatech). Heart mitochondria (0.8 mg) and substrates for the different assays, namely glutamate-malate (5 mM and 2.5 M) and succinate (5 mM) were added into a reaction medium containing 130 mM sucrose, 50 mM KCl, 2.5 mM KH_2PO_4, 5mM HEPES, 2 mM $MgCl_2$ (pH 7.4) under constant stirring. For complex II-assays, succinate was added with rotenone (3 M) to inhibit complex I. The respiratory parameters included: state 2 and state 3 determined before and after adding ADP (156 nmol/mg), respectively, and state 4 measured as the rate of oxygen consumption after ADP phosphorylation. The respiratory control ratio (RCR) was

calculated as the ratio between state 3 and state 4, while the ADP/O was calculated as the number of nmol ADP phosphorylated by natom O_2 consumed [103].

III. Mitochondrial transmembrane electrical potential assays

Mitochondrial transmembrane electric potential (Δψ) was indirectly monitored based on the activity of the lipophilic cation tetraphenylphosphonium (TPP+), using a TPP+-selective electrode as previously described [104, 105] in combination with a silver chloride reference electrode (Tacussel, Model MI 402, France). The TPP+ and the reference electrode were inserted in an open chamber, connected to a pH meter (Jenway, Model 30505, UK). The obtained signals were transferred to a potentiometric recorder (Kipp & Zonen, Model BD 112, Holland). Δψ was estimated as indicated by Kamo et al. (1979) through the equation: $\Delta\psi = 59 \log(\nu/V) - 59 \log(10^{\Delta E/59} - 1)$, where ν, V, and ΔE stand for mitochondrial volume, volume of the incubation medium, and deflection of the electrode potential from the baseline, respectively. A matrix volume of 1.1 µL/mg of protein was assumed and no correction was made for the "passive" binding to the mitochondrial membranes, since the purpose of the experiments was to show relative changes rather than absolute values. Heart mitochondria (0.8 mg) were incubated in a reaction medium containing 100 mM KCl, 100 mM sucrose, 10 µM EGTA, 2 mM KH2PO4, and 5 mM Hepes (pH 7.4), supplemented with 3 µM TPP+. The measurement of complex-I and complex II-linked with substrates energization was performed with glutamate-malate (5 mM and 2.5 mM, respectively) or succinate (5 mM) plus rotenone (3 M) and depolarization was achieved by adding ADP (156 nmol/mg).

6. Histology

The LV and gastrocnemius muscle were manually processed, fixed for 24 hours in formol, dehydrated in solutions with increasing concentrations of ethanol, diafined for 2 hours in xylol and impregnated in paraffin (2 hours). After paraffin embedding, 3 µm muscle sections were sliced in a rotative microtome (model RM2125 RTS, Leica, Germany). Muscle sections were dewaxed, rehydrated and subsequently stained with HE solution to assess cardiomyocyte area. Briefly, sections were dewaxed in xylol, hydrated in ethanol and stained by Harris haematoxylin during 5 minutes, placed in tap water, stained in alcoholic eosin for 5 minutes, dehydrated in ethanol, dewaxed in xylol and mounted with Entellan®. An optic microscope (Leitz Wetzlar – Dialux 20, Wetzlar, Germany), equipped with a photographic camera (Olympus XC30, Tokyo, Japan) and

with a 25x objective was used to visualize and photograph the histological preparations. The area of 60 cardiomyocytes per animal was calculated through Cell^B software (Olympus).
Picrosirius Red staining was used to quantify myocardial fibrosis. Briefly, sections were dewaxed in xylol, hydrated in ethanol until running water, stained with Picrosirius Red 0.1% solution for 1.5 hours immersed for 2 seconds in acidified water at 0.5%, dehydrated in ethanol at 100% during 5 minutes (3 times), dewaxed in xylol and mounted with Entellan®. Eight fields per animal were photographed with a digital camera (Olympus XC30) coupled to an optic microscope (Leitz Wetzlar – Dialux 20) with a 10x objective. Latter, images were analysed with Image Pro Pus 6 software (Media Cybernetics, Rockville, USA) to calculate the area of fibrosis.

7. Electron Microscopy

After tissues harvest, the samples were immediately fixed in 2.5% gluteraldehyde in cacodylate buffer and the subsequently post-fixated was done in osmium tetroxide. The samples were then dehydrated in increasing ethanol solutions (95–100%) and subsequently embedded in a mixture of polypropylene oxide with Epon resin at room temperature. Subsequently samples were placed in Epon resin blocks at 60°C for 2 to 3 days. Ultrathin sections (50–60 nm) were obtained and collected on copper grids, stained with uranyl acetate, citrate and finally examined under a transmission electron microscope (JEM1400, USA) with a 10000, 20000 and 30000x magnification. To assess mitochondrial morphological parameters, such as number of mitochondria, area of mitochondria and its circularity. Images were analysed with ImageJ (Version 1.49b).

8. Force measurements in isolated cardiomyocytes

Force measurements were performed in single, mechanically isolated cardiomyocytes as described previously [106] using a force transducer from Aurora Scientific Inc. (Model 403A) and a length controller (Model 315C-I). The software used for data and real time image acquisition was ASI 600A and VSL 900B, respectively.

I. Sample preparation

Samples from the heart apex (1.5 mg wet weight) (Sh=10, Ba=15, Deb=10) were defrosted in 2.5 mL of Ca^{2+}-free relaxing solution (Appendix B) at 4°C degrees and cut in small pieces. After

a potter-based mechanical disruption with pestle and a rotor, (3-5 seconds at 1200 rpm for 3 times, Plastilab Kastell 6105, Terre Haute Glas-col, GKH GT Motor Control), the resulting cardiomyocytes suspension was incubated with 0.5% Triton X-100 for 5 minutes at room temperature to permeabilize the membranes. Later, cells were washed with relax solution and centrifuged (1500 rpm, 1 min, 4°C). This procedure was repeated 4 to 5 times until total removal of the detergent.

II. Force measurements

Cardiomyocytes suspension was visualized under a microscopic (Olympus IX51) to choose the elongated cells with a uniform pattern of striation. The selected cardiomyocyte was attached between a force transducer and a length motor with aquarium silicone adhesive for approximately of 50 minutes. Cardiomyocytes were visualized with a magnification of 10-20x with a video-camera CCD (UEye) and with VSL software (ASI, aurora Scientific Inc., Model 900B). The cardiomyocyte was transferred to a 60µL well filled with relaxing solution (Appendix B). The cell was stretched until a sarcomere length of 2.2 µm and passive tension measured during this process in order to construct a passive tension-length relation. With a sarcomere length (SL) at 2.2 µm, the cardiomyocytes were subjected to both relaxing and Ca^{2+} activating solutions with a pCa ($-\log_{10}[Ca^{2+}]$) ranging from 9.0 (relaxing) to 4.5 (maximal activation) to produce a force-pCa relation. Maximal activation at pCa 4.5 was used to calculate maximal calcium-activated isometric force. After transferring the cardiomyocyte from relaxing to activating solution, isometric force started to develop (Total tension, Tt). Once a steady-state force level was reached, the cell was shortened for 1 ms to 80% of its original length (slack test) to determine the baseline of the force transducer. The distance between the baseline and the steady force level is Tt. After 20 ms, the cell was re-stretched and returned to the relaxing solution, in which a second slack test of 10-second duration was performed to determine passive tension (Tp). The slack test at pCa=4.5 allowed to measure the rate of force-redevelopment (Ktr), since this manoeuvre resulted in the complete dissociation of cross-bridges from actin, so that the subsequent redevelopment of tension was related to the rate of cross-bridge reattachment. Finally the cell was activated again with the saturating calcium solution (pCa=4.5) to check for the cardiomyocyte functional stability at the integrity of the protocol. Finally the dimensions of the cell were measured and the force values were normalized to the cardiomyocyte cross-sectional area. Data acquisition was done by ASI 600A program with a sampling frequency of 2 KHz.

9. Protein analysis by Western Blot

Left ventricular tissue was homogenized in RIPA buffer and protein concentrations were determined according to Bradford's method. After the addition of *Laemmli buffer* (1 M Tris-HCl pH 6.8, 10% SDS, 20% glycerol, 0.004% bromophenol blue, 20% 2-mercaptoetanol) 20 μg of protein were separated by SDS-PAGE (Mini-PROTEAN Tetra Cell, Bio-Rad) at 150V for an hour. After transferring to a nitrocellulose membrane (Bio-Rad 1620115 and 1620112) and blocking with 5% BSA (w/v) in TBS-Tween 20 (Tris-buffered saline-Tween 20) the membranes were incubated with primary antibodies overnight at 4°C (eNOS (Santa Cruz, sc-376751) p-eNOS (Santa Cruz, sc-12972), iNOS (Abcam, ab323), p-iNOS (Abcam, ab204017) MFN1 (Cell Signalling, 14739), MFN2 (Cell Signalling, 9482), PGC1-α (Cell Signalling, 2178), Bax (Cell Signalling, 2772), BCL-2 (Cell Signalling, 2876) NCX (Santa Cruz ,sc-32881), p38 (Cell Signalling, 9212), p-p38 (Cell Signalling, 9211), AKT (Cell Signalling, 9272), p-AKT (Cell Signalling, 9271), mTOR (Cell Signalling, 2972), p-mTOR (Cell Signalling, 2971), GKK3β (Cell Signalling, 9315), p-GSK3β (Cell Signalling, 9331), SERCA-2A (Cell Signalling, 4388); PLB (Thermo-Fisher, MA3-922), p-PLB (cell signalling, 8496). Finally, membranes were incubated for an hour at room temperature with secondary antibodies conjugated with a fluorescent molecule (IRDye 800CW and IRDye 680LT) against rabbit, mouse or goat. The signal was detected by an image acquisition system (Odyssey Infrared Imaging System LI-COR Biosciences at 700 or 800 nm). The values were normalized to Ponceau-S and to the average values of sham group.

10. Glutathione measurements/quantification

Glutathione (GSSG/GSH) (ADI-900-160, ENZO) were measured in cardiac tissue according to manufacture instructions.

11. Gene expression quantification – Real time quantitative Polymerase Chain Reaction (RT-qPCR)

I. RNA extraction

RNA was extracted as described with minor modifications. Briefly, 500 μL of Tripure (Roche) and 300 mg of Bulk Beads (Ø 1.4 mm zirconium oxide beads, Precellys) were added to each tissue sample. Cell disruption was achieved by performing three cycles of 6500 rpm, for 30

seconds, in MagNALyser (Roche). Then, 100 µL of chloroform was added and the mixture was centrifuged for 15 minutes at 4°C at 15000 rpm. Aqueous phase was removed to a new tube and RNA was precipitated with 500 µL of isopropanol, incubated at room temperature for 10 minutes. Following a 10 minutes centrifugation at 15000 rpm at 4°C, supernatant was discarted and RNA pellet was washed with 70% ethanol. RNA was ressuspended in 50 µL of milliQ water. Concentration and quality of extracted RNA was assessed by measuring the absorvance at 260 nm (A_{260}) and 280 nm (A_{280}) in a Nanodrop 2000c (Thermo Scientific).

II. Transcriptase reverse reaction

A mixture of 500 ng Oligo $(dT)_{12-18}$, 1000 ng RNA, 500 uM dNTP Mix and milli-Q water was heated at 65°C for 5 minutes and quickly chill on ice. After additing 4 µL of 5X First-Strand Buffer, 2 µL of 0.1 M DTT and 1 µL of rRNAsin (40 units/µL) the mixture was incubated at 42°C for 2 minutes. Transcriptase reverse reaction was carried out by adding 1µL of SuperScript™ II RT (200 units, Invitrogen) at 42°C for 50 minutes. Reaction was inactivated by heating at 70°C for 15 minutes.

III. Gene expression analysis

Expression for the genes listed below was quantified comparatively for the three animal groups: Sham, banding and debanding. GAPDH was used as the house-keeping gene since its complementary DNA (cDNA) levels were similar in all the studied groups. Results of gene expression for each animal were normalized for the average of the sham group. Equal amounts of (cDNA (100 ng/µL)) from every sample underwent real-time qPCR (StepOne Plus, Applied Biosystems) experiments for each gene and reactions were prepared as described in SensiFAST™ SYBR Hi-ROX kit (Bioline). Briefly, reaction contains 1x SensiFAST SYBR Hi-ROX Mix, 400 nM forward primer, 400 nM reverse primer, 5 ng template for a final volume of 20 µl. Two step PCR program was carried out, a first cycle of 95°C for 2 minutes, followed by 40 cycles, comprising a first step at 95°C for 5 seconds and a second step at 60°C for 30 seconds. Nucleotide sequence of the primers used are described in **Table 1**.

Real-time PCR data were analyzed using the comparative CT method:

$$2^{-\Delta Ct}\,\text{Disease} / 2^{-\Delta Ct}\,\text{Control} = 2^{-(\text{Ct gene of interest} - \text{Ct } \textit{GAPDH})} / 2^{-(\text{Ct gene of interest} - \text{Ct } \textit{GAPDH})}$$

Table 1: PCR primer pairs used for gene expression quantification.

Gene	Sequence 5´→ 3´	Tissue
GAPDH		CM, SM
Forward	TGGCCTTCCGTGTTCCTACCC	
Reverse	CCGCCTGCTTCACCACCTTCT	
PDK4		CM, SM
Forward	CGAGCATCAAGAAAACCGCC	
Reverse	AGCAGTGGAGTATGTGTAAC	
CPT1		CM, SM
Forward	TGGGCGACAGGCATTTTTTT	
Reverse	CTGGACAGGAGACGAACA	
GLUT4		CM, SM
Forward	AGGCCGGGACACTATACCC	
Reverse	TCCCCATCTTCAGAGCCGAT	
GLUT1		CM, SM
Forward	GCTGGCTTCTCTAACTGGACC	
Reverse	GTGATGGAGGACAGTGGTGAT	
COL1A1		CM
Forward	GCTTTAGCCTCCTGGCAGAT	
Reverse	GAGATGGTGGGAGAGGGTCA	
COL3A1		CM
Forward	AGGGAGAATTCAAGGCTGAAGG	
Reverse	TGCCACCCTATGTGAAAAGACA	

CM, Cardiac muscle; SM, Skeletal muscle.

12. Statistical analysis

Results are expressed as mean ± SEM. Statistical analysis was performed using GraphPad Prism software. Comparisons were performed by One- or Two-Way ANOVA and appropriate post-hoc test were used. The probability values <0.05 were taken as significant.

RESULTS

a) Morphometric characterization

As depicted in **Table 2**, the morphometric data revealed a significant increase in heart weight and LV plus septum in banding relative to sham animals. The same variation is observed in right ventricle, showing that lung congestion, observed in Ba group, is already imposing a certain degree of RV overload. After removing the constriction, we observed a normalization of all these parameters in the Deb group.

The gastrocnemius muscle weight decreased significantly in banding relative to sham group, revealing muscle atrophy, which partly recovered after debanding.

The mortality rate associated to the surgical procedure of debanding was of 33%.

Table 2: Morphometric data.

	Sh (n=10)	Ba (n=15)	Deb (n=10)
HW/BW (g/g)	2.937 ± 0.246	3.618 ± 0.193$^{\alpha}$	2.948 ± 0.120$^{\chi}$
LV+S/BW (mg/g)	1.386 ± 0.144	2.250 ± 0.119$^{\alpha\alpha\alpha}$	1.464 ± 0.144$^{\chi\chi}$
Lungs/BW (g/g)	4.300 ± 0.117	4.821 ± 0.168$^{\alpha}$	4.316 ± 0.101$^{\chi}$
RV/BW (g/g)	0.450 ± 0.012	0.541 ± 0.030$^{\alpha\alpha}$	0.454 ± 0.013$^{\chi\chi}$
Gastrocnemius (g)	2.302±0.193	1.765±0.066$^{\alpha}$	2.073±0.109

HW**, heart weight; **BW**, body weight; **LV+S**, left ventricle plus sept; **RV**, right ventricle.* Values are mean ± SE, One-way anova; ***Ba/Deb vs Sh*:** α, p<0.05; αα, p< 0.01; ααα, p<0.001; ***Deb vs Ba: χ, p<0.05; χχ, p<0.01, χχχ, p< 0.001.

b) Echocardiographic characterization

In order to characterize the heart function of these animals, an echocardiography evaluation was performed (**Table 3**). This evaluation revealed that, despite the absence of differences of body surface area and weight among all the experimental groups (sham, banding and debanding), LV wall thickness increased and cavity dimensions decreased in banding compared to sham animals, denoting concentric hypertrophy, typical of HFpEF. As expected, after overload relief, this phenotype reversed partially. Indeed, the normalization of LV cavities in systole and diastole allowed to increase end diastolic volumes in debanded rats. In addition to concentric LV remodelling, diastolic dysfunction was observed in banding rats, as evidenced by the significant decrease of the E/A and the increased E/E´ ratios. Moreover, as a consequence of the increased filling pressures observed in banding rats, the velocities of A wave increased and left and right atria dilated. Curiously, after aortic-constriction removal, the atria area did not return to sham values. In RV we did not observe any increase in TAPSE in debanding despite its reduction in banding group. The reduction in TEI index in banding animals, denotes a worse cardiac performance in this group. However, this parameter normalized in the debanded rats. In addition to diastolic dysfunction, typical of HFpEF, the banding animals also presented systolic abnormalities, as observed by

decreased S' and FS. While the former normalized after debanding the latter did not. All the changes observed in banding rats together with the preservation of EF, confirmed the usefulness of aortic banding as an animal model to study HFpEF.

Table 3: Echocardiography evaluation.

	Sh (n=10)	Ba (n=15)	Deb (n=10)
Weight (kg)	0.388±0.006	0.401±0.100	0.397±0.010
BSA (cm^2)	4.873±0.035	4.947±0.080	4.916±0.080
AWd (cm)	0.143±0.006	0.202±0.005$^{\alpha\alpha\alpha\alpha}$	0.168±0.010$^{\chi\chi}$
LVd (cm)	0.743±0.013	0.696±0.014$^{\alpha}$	0.769±0.016$^{\chi\chi}$
PWd (cm)	0.138±0.007	0.206±0.008$^{\alpha\alpha\alpha\alpha}$	0.166±0.008 $^{\alpha\chi\chi}$
AWs (cm)	0.220±0.005	0.306±0.008$^{\alpha\alpha\alpha\alpha}$	0.252±0.012 $^{\alpha\chi\chi}$
LVs (cm)	0.448±0.025	0.383±0.013$^{\alpha}$	0.467±0.029$^{\chi\chi}$
PWs (cm)	0.216±0.005	0.307±0.011$^{\alpha\alpha\alpha\alpha}$	0.263±0.010 $^{\alpha\alpha\chi}$
LVMass (g)	0.688±0.035	1.070±0.032$^{\alpha\alpha\alpha\alpha}$	0.908±0.037 $^{\alpha\alpha\chi\chi}$
EDVI (µL/cm^2)	187.119±8.217	165.833±8.434$^{\alpha}$	205.797±13.445$^{\chi\chi}$
ESVI (µL/cm^2)	42.437±4.727	29.874±2.797$^{\alpha}$	50.469±8.388$^{\chi\chi}$
HR (bpm)	376±13	349±9	340±12$^{\alpha}$
E' (m/s)	0.075±0.004	0.061±0.002$^{\alpha\alpha}$	0.074±0.004$^{\chi\chi}$
E (m/s)	0.985±0.040	1.108±0.040	1.074±0.048
A (m/s)	0.646±0.044	0.812±0.039$^{\alpha}$	0.691±0.086
E/A	1.547±0.074	1.354±0.041$^{\alpha}$	1.571±0.107$^{\chi}$
E/E'	13.456±0.694	18.635±0.995$^{\alpha\alpha}$	14.667±0.702$^{\chi}$
S' (m/s)	0.060±0.003	0.043±0.002$^{\alpha\alpha\alpha\alpha}$	0.054±0.002$^{\chi\chi}$
TEI Index (ms)	0.518±0.017	0.396±0.016 $^{\alpha\alpha\alpha\alpha}$	0.509±0.026$^{\chi\chi}$
EF (%)	78.288±2.906	73.849±4.228	74.541±3.162
FS (%)	46.879±1.146	40.943±1.130$^{\alpha\alpha}$	41.147±2.702$^{\chi}$
LAA (cm^2)	0.314±0.015	0.421±0.021$^{\alpha\alpha\alpha}$	0.370±0.011$^{\alpha}$
RAA (cm^2)	0.207±0.006	0.246±0.009$^{\alpha\alpha}$	0.254±0.009$^{\alpha\alpha}$
TAPSE (cm)	0.306±0.009	0.230±0.013$^{\alpha\alpha\alpha}$	0.257±0.008$^{\alpha}$

BSA, body surface area*;* ***AWd,*** anterior wall in diastole*;* ***LVd,*** left ventricle cavity in diastole*;* ***PWd***, posterior wall in diastole**;** ***AWs***, anterior wall in systole*;* ***LVs***, left ventricle cavity in systole*;* ***PWs***, posterior wall in systole*;* ***LVMass***, left ventricle mass; ***EDVI***, end-diastolic volume index; ***ESVI***, end- systolic volume index; ***HR***, heart rate; ***E´***, wave velocity of tissue Doppler at the lateral mitral annulus; ***E,*** peak of pulse Doppler wave of early mitral flow velocity**;** ***A,*** peak of pulse Doppler wave of late mitral flow velocity**;** ***E/A,*** ratio between peak E and A waves; ***E/E'*** ratio between E and E' waves; ***S´,*** peak systolic velocity; ***TEI index***, myocardial performance index; ***EF***, ejection fraction; ***FS***, fractional shortening; ***LAA***, left atrium area; ***RAA***, right atrium area; ***TAPSE***, tricuspid annular plane systolic excursion. Values are mean ± SEM. One Way-Anova, ***Ba/Deb vs Sh*****:** α, p<0.05; αα, p< 0.01; ααα, p<0.001; ***Deb vs Ba:*** χ, p<0.05; χχ, p<0.01, χχχ, p< 0.001.

c) Cardiomyocyte hypertrophy

In cardiac muscle, aortic constriction induced as expected an increase of cardiomyocyte area relative to sham animals (**Figures 3A and 3E**) (Sh=255.1±14.1, Ba=468.3±17.7, p<0.0001), highlighting hypertrophy at the cardiomyocytes level in banding rats. After removal of the aortic constriction we observed a partial reduction of the cardiomyocyte area (Sh=255.1±14.1, Ba=468.3±17.7, Deb=375.8±12.7, Sh vs Ba, p=0.0012; Ba vs Deb, p<0.001). Since AKT activation induces cardiac hypertrophy, partly mediated by the reduction of the anti-hypertrophic action of GSK3-β and by increased activation of mTOR, we decided to explore this pathway in the context of the present work. We observed augmented AKT activation (Sh=100±4, Ba=148±11, p=0.03) and a tendency to increase both GSK3-β and mTOR phosphorylation in banding rats when compared to sham animals (**Figures 3B, C and D**) (GSK3-β: Sh=100±5, Ba=159±18, p=0.08; mTOR: Sh=100±4, Ba=125±6, p=0.07). When the constriction was relieved, we observed a concomitant reduction of AKT and (a tendency) of mTOR phosphorylation but not in GSK3-β. (AKT: sh=100±4; Ba=148±11; Deb=91±14, Sh vs Ba p=0.03; Ba vs Deb, p=0.01. mTOR: Sh=100±4, Ba=125±6, Deb=102±8, Sh vs Ba p=0.07; Ba vs Deb p=0.06; GSK3-β: Sh=100±5, Ba=159±18, Deb=157±34, Sh vs Ba p=0.08), indicating that debanding procedure did not significantly impact the GSK3-β anti-hypertrophic activity.

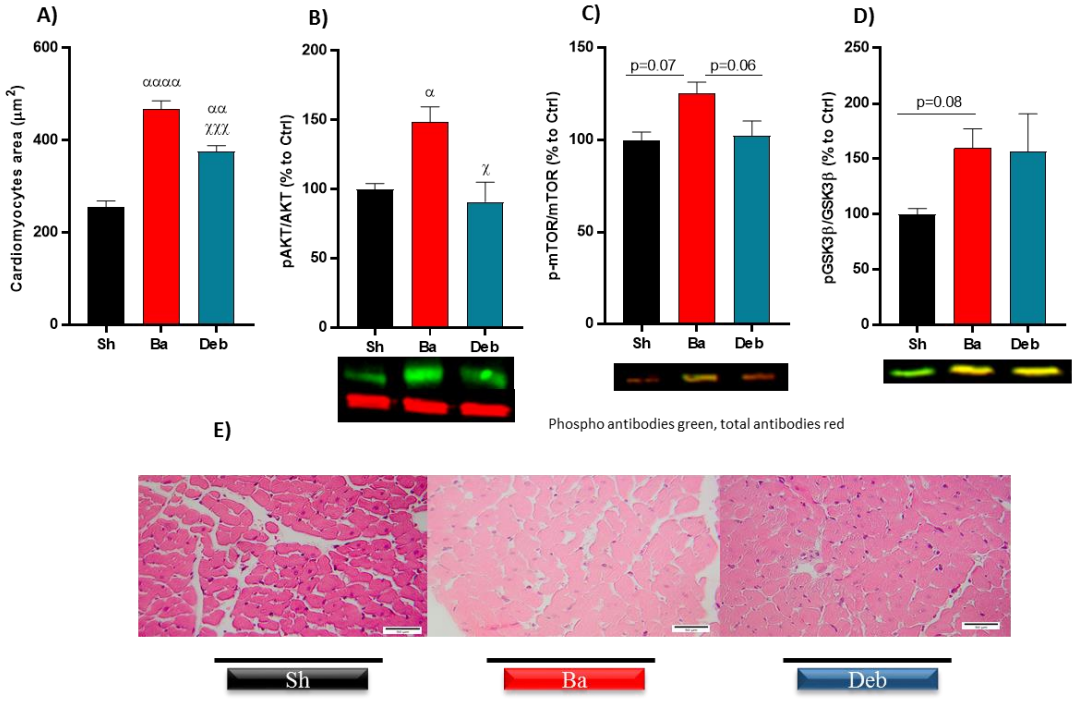

Figure 3- Effect of pressure overload on left ventricular hypertrophy. ***A)*** Cardiomyocytes area evaluated by histology; Western blot relative quantification of: ***B)*** ratio of phosphorylated to total AKT; ***C)*** ratio of phosphorylated to total mTOR; ***D)*** ratio of phosphorylated to total glycogen synthase kinase 3 beta; ***E)*** representative images of histological samples. n=5 for each group. Representative western blot lanes, phospho antibodies are in green, total antibodies are in red. Values are mean ± SEM, One-way anova. ***Ba/Deb vs Sh*****:** α, p<0.05; αα, p< 0.01; ααα, p<0.001; ***Deb vs Ba*****:** χ, p<0.05; χχχ, p< 0.001.

d) Myocardial stiffness

It is well accepted, and observed in our banding rats that myocardial stiffness increases in concentric hypertrophy and HFpEF, so we decided to evaluate the cardiomyocyte and extracellular matrix contribution. Our data revealed an increase of myocardial fibrosis in banding relative to sham group (Sh=8.79±0.66; Ba=14.6±1.0, p<0.001). Moreover, the debanding procedure did not reduced fibrosis (Sh=8.79±0.66; Deb=13.92±0.56, p=0.003) (**Figures 4A and B**). Regarding TGF-β, this cytokine was significantly increased in banding relative to sham animals (Sh=1.0±0.3; Ba=2.0±0.2, p=0.04), however, after constriction relief, TGF-β expression decreased (Ba=02.0±0.2; Deb=1.3±0.3, p=0.13) (**Figure 4C**). The expression levels of procollagen type I and type III increased in banding relatively to the sham group (Sh=1.0±0.1; Ba=1.6±0.2, p=0.04; Sh=1.0±0.2; Ba=1.6±0.2, p=0.04, respectively) and normalized after constriction removal (Sh=1.0±0.1; Deb=0.9±0.1, p=0.90; Sh=1.0±0.2; Deb=0.7±0.1, p=0.67, respectively) (**Figures 4D and E**).

It is well recognized that titin isoforms and its phosphorylation status contributes greatly to myocardial changes in passive tension. Not surprisingly, we observed an increase in titin

phosphorylation in banding rats compared to sham (Sh=100±14; Ba=153±10, p=0.04), particularly in titin's PEVK segments (Sh=100±18; Ba=198±21, p=0.03) (**Figures 4F, G and H**). In the debanding group we observed a reduction of titin and its PEVK segment phosphorylation, but not to the same extent as the sham group (Ba=152.9±9.8; Deb=127.3±12.86, p=0.317; Ba=152.9±9.8; Deb=127.3±12.86; p=0.317, respectively) (**Figures 4F, G and H**). Since titin is a major determinant of cardiomyocyte passive tension, we compared the passive force in isolated cardiomyocytes in our rats at different sarcomere lengths (**Figure 4I**). When compared to sham, banding rats displayed an increased stiffness, as observed by a steeper passive tension versus SL relation, that partially reversed in the debanding group, only significant for higher SL (Ba=7.12±0.37; Deb=6.25±0.47, p=0.05) (**Figure 4I**).

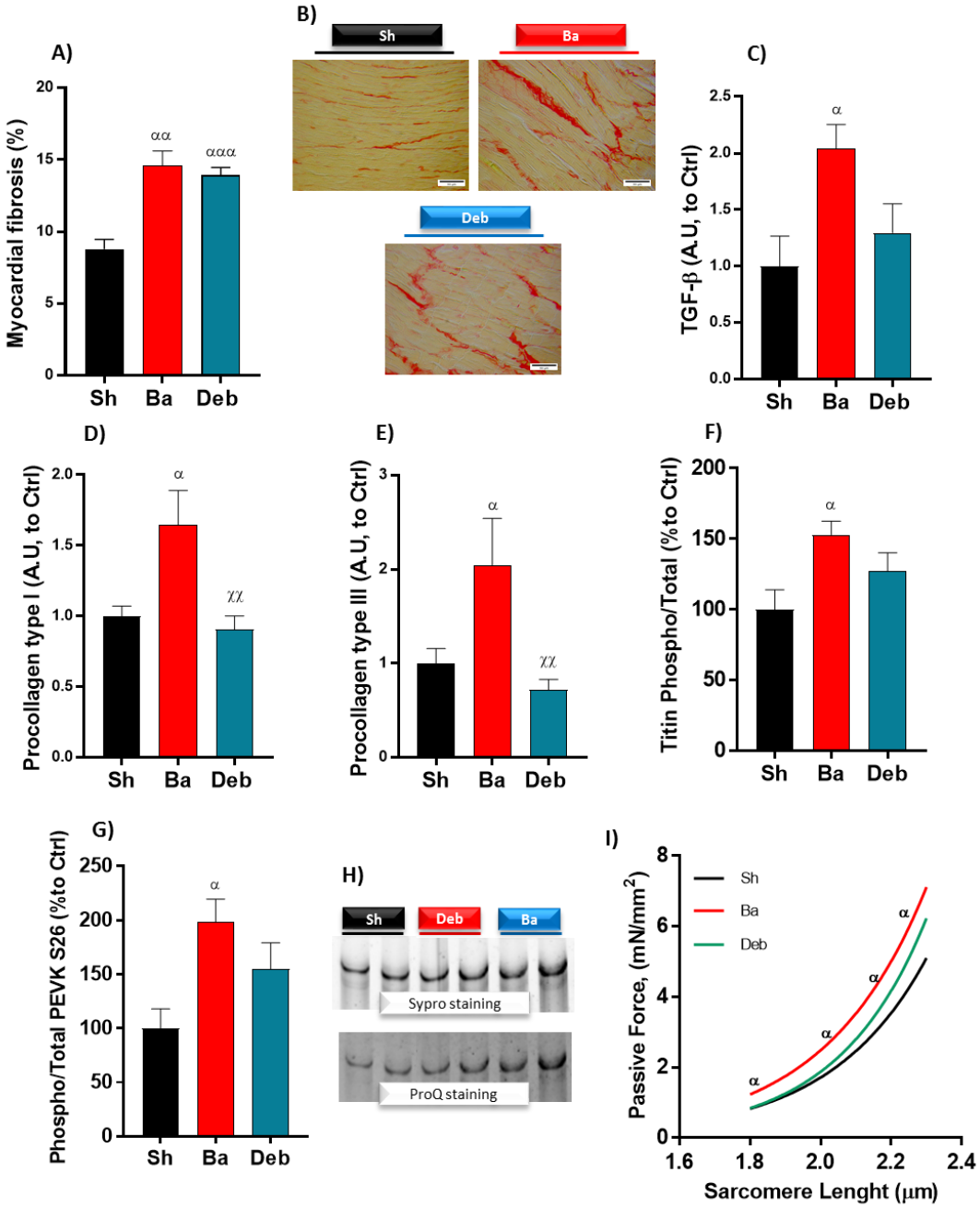

Figure 4- Effect of pressure overload on ventricular stiffness. ***A)*** Cardiomyocytes passive tension; ***B)*** myocardial fibrosis assessed in Red-Sirius-stained sections; ***C)*** representative images of histological samples; ***D)*** ratio of phosphorylated to total Titin; ***E)*** ratio of S26 phosphorylation to total Titin PEVK segment; ***F)*** representative images**;** ***G)*** expression of procollagen type I; ***H)*** expression of procollagen type III**.** n=7 for each group. Values are mean ± SEM, Two-way Anova for passive tension: ***Ba/Deb vs Sh*****:** α, p<0.05; αα, p< 0.01; ααα, p<0.001; ***Deb vs Ba:*** χχ, p<0.01.

e) Cardiomyocyte force, calcium sensitivity and homeostasis

Considering the role of calcium in contractility, we evaluated cardiomyocytes' active tension and calcium sensitivity. Both parameters were altered in banding animals when compared to sham (**Figures 5A and B**), since active tension (Sh=15.78±1.48; Ba=24.73±2.56, p=0.04), and calcium sensitivity increased (Sh=5.678±0.021; Ba=5.374±0.093, p=0.0062). In debanding animals a partial improvement of these parameters was observed, since debanding was not significantly different from banding (Ba=24.73±2.56; Deb=20.52±1.91, p=0.3282) (Ba=5.374±0.093; Deb=5.535±0.037, p=0.3616). The cooperativity of the myofilaments (nHill) increased (Sh=1.528±0.201; Ba=3.378±0.273, p<0.001, **Figure 5C**) and the rate constant for force redevelopment (ktr), measuring the rate of cross-bridge entry into the force generating state, decreased (Sh=4.751±0.403; Ba=3.629±0.264, p=0.031) in banding rats (**Figures 5D**). After debanding, while the cooperativity of the myofilaments recovered completely (Sh=1.528±0.201; Ba=3.378±0.273; Deb=2.058±0.146, Sh vs Ba p=0.4307; Ba vs Deb p=0.0013, **Figure 5C**), Ktr remained lower (Sh=4.751±0.403; Deb=3.379±0.163; p=0.01, **Figure 5D**). To evaluate myocardial calcium homeostasis, we evaluated some proteins such as SERCA-2a, PLB and NCX by Western Blot. Regarding SERCA-2a expression, we observed its significant reduction in banding relative to sham animals (Sh=100±24; Ba=29±6, p=0.005, **Figure 5E**). The ratio of p-PLB/PLB only showed a trend to decrease in the banding group when compared to sham (Sh=100±12; Ba=33±56; p=0.10, **Figure 5F**). Altogether, these abnormalities denote an impaired calcium reuptake to sarcoplasmic reticulum. Removal of aortic constriction improved SERCA-2a content up to the level of the Sh group (Sh=100±15; Ba=42±10; Deb=73±22, Sh vs Deb p=0.41; Ba vs Deb p=0.37). Moreover, the ratio p-PLB/PLB values increased significantly in debanding animals when compared to banding and sham, denoting an increase of phospholamban phosphorylation and subsequently a decrease of SERCA inhibition. (Sh=100±12; Ba=33±6; Deb=220±61; Sh vs Deb p=0.014; Ba vs Deb p<0.001). NCX was significantly reduced in banding animals when compared to sham animals (Sh=100±4; Ba=37±9, p=0.01, **Figure 5G**), denoting an impaired calcium transport out of the cardiomyocyte. This reduction was attenuated after overload relief (Ba=37±9; Deb=72±17, p=0.322).

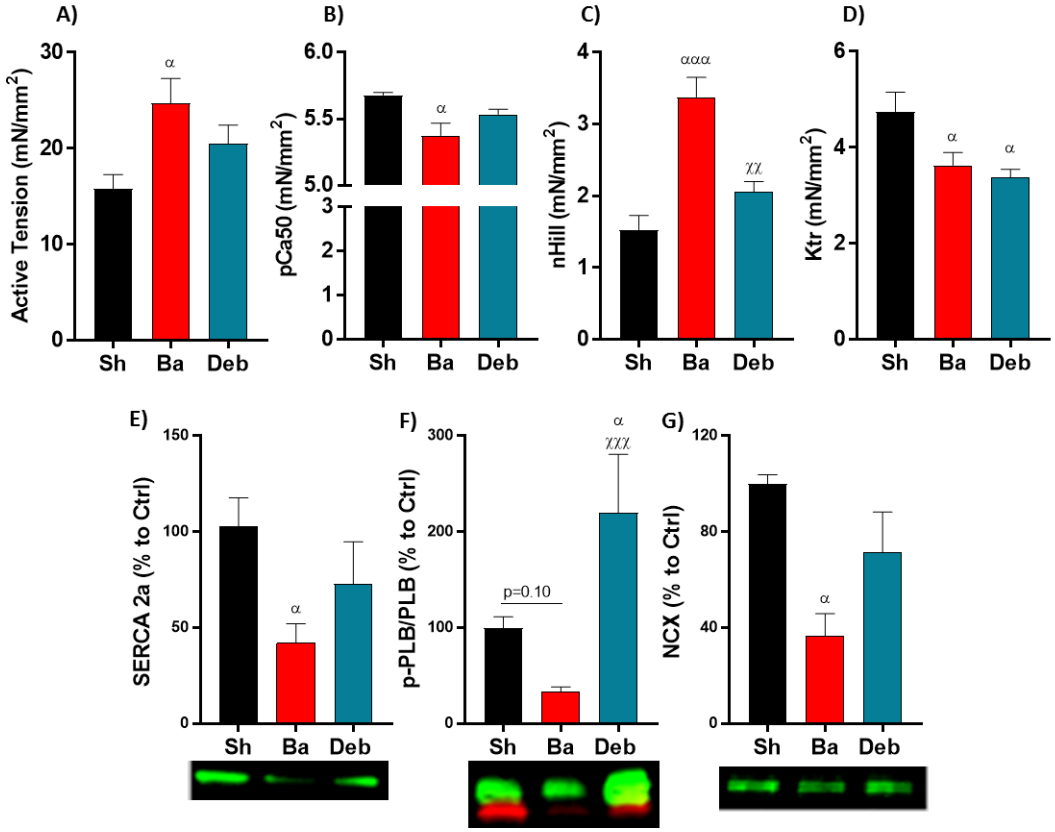

Figure 5- Effect of pressure overload on calcium. ***A)*** Cardiomyocytes active tension; ***B)*** myofilaments calcium sensitivity; ***C)*** *Hill*-coefficient; ***D)*** the rate of tension redevelopment; **Western blot relative quantification:** ***E)*** sarcoplasmic/endoplasmic reticulum Ca^{2+}ATPase 2a (SERCA-2a); ***F)*** ratio of phosphorylated to total phospholamban; ***G)*** sodium-calcium exchanger. Representative western blot lanes, phospho antibodies are in green, total antibodies are in red. Values are mean ± SEM. One Way-Anova: ***Ba/Deb vs Sh*****:** α, $p<0.05$; ααα, $p<0.001$; ***Deb vs Ba:*** χχ, $p<0.01$, χχχ, $p< 0.001$.

f) Nitric oxide, oxidative damage and antioxidant enzymes

In order to assess the status of myocardial NOS, we evaluated the phosphorylation of eNOS and total iNOS by Western Blot (**Figures 6A and B**). The ratio of phosphorylated to total eNOS and iNOS were changed in banding animals compared to sham, however while the former decreased, the latter increased (eNOS, Sh=100±3; Ba=62±10; p=0.01; iNOS, Sh=100±18; Ba=202±13; p=0.009). These changes normalized after the debanding procedure (eNOS, Ba=62±10; Deb=87±6, p=0.011; iNOS, Ba=202±13; Deb=121±15, p=0.008). Additionally, anti-oxidant enzymes, such as catalase and glutathione were quantified to assess myocardial redox status. Regarding catalase we denoted a significant raise in banding relative to sham group (Sh=100±12; Ba=135±9, p=0.05, **Figure 6C**). When the aortic constriction was removed, catalase values partially recovered (Ba=135±9; Deb=105±1, p=0.11). The levels of glutathione showed a trend to be reduced in banding rats when compared to sham (Sh=131±12; Ba=103±6; p=0.07, **Figure 6D**). Moreover, the levels of reduced glutathione and the ratio of reduced to oxidize was significantly reduced in banding rats (GSH, Sh=121±1; Ba=93±1, p<0.0001; GSH/GSSG, Sh=11.6±0.3; Ba=9.5±0.3; p<0.001, **Figures 6E and F**). In debanding, we denoted an improvement of anti-oxidant enzymes as assessed by the increase of reduced glutathione (Sh=121±1, Deb=108±8, p<0.001) but not enough to be equal to sham animals (Ba=93±1, Deb=108±8, p<0.001, **Figure 6E**). Moreover, the ratio of reduced to oxidize glutathione increased (Ba=9.5±0.3, Deb=12.6±0.1, p<0.001, **Figure 6F)**

In adult myocytes p38 activity can contribute to pathological hypertrophy and remodeling and can also phosphorylate Bax and trigger apoptosis. In banded animals we observed an increase of the ratio of both p-p38/p38 as well as Bax/Bcl-2 (p-p38/p38, Sh=100±10; Ba=3920±1428, p<0.001; Bax/Bcl-2, Sh=100±4; Ba=350±69; p=0.004). When the aortic constriction was removed despite the reduction of p-p38/p38 (Ba=3920±1428; Deb=131±36, p<0.001, **Figure 6G**) the ratio of Bax/Bcl-2 remained higher when compared to sham (Sh=100±4; Deb=282.3±13.1, p=0.04, **Figure 6H**).

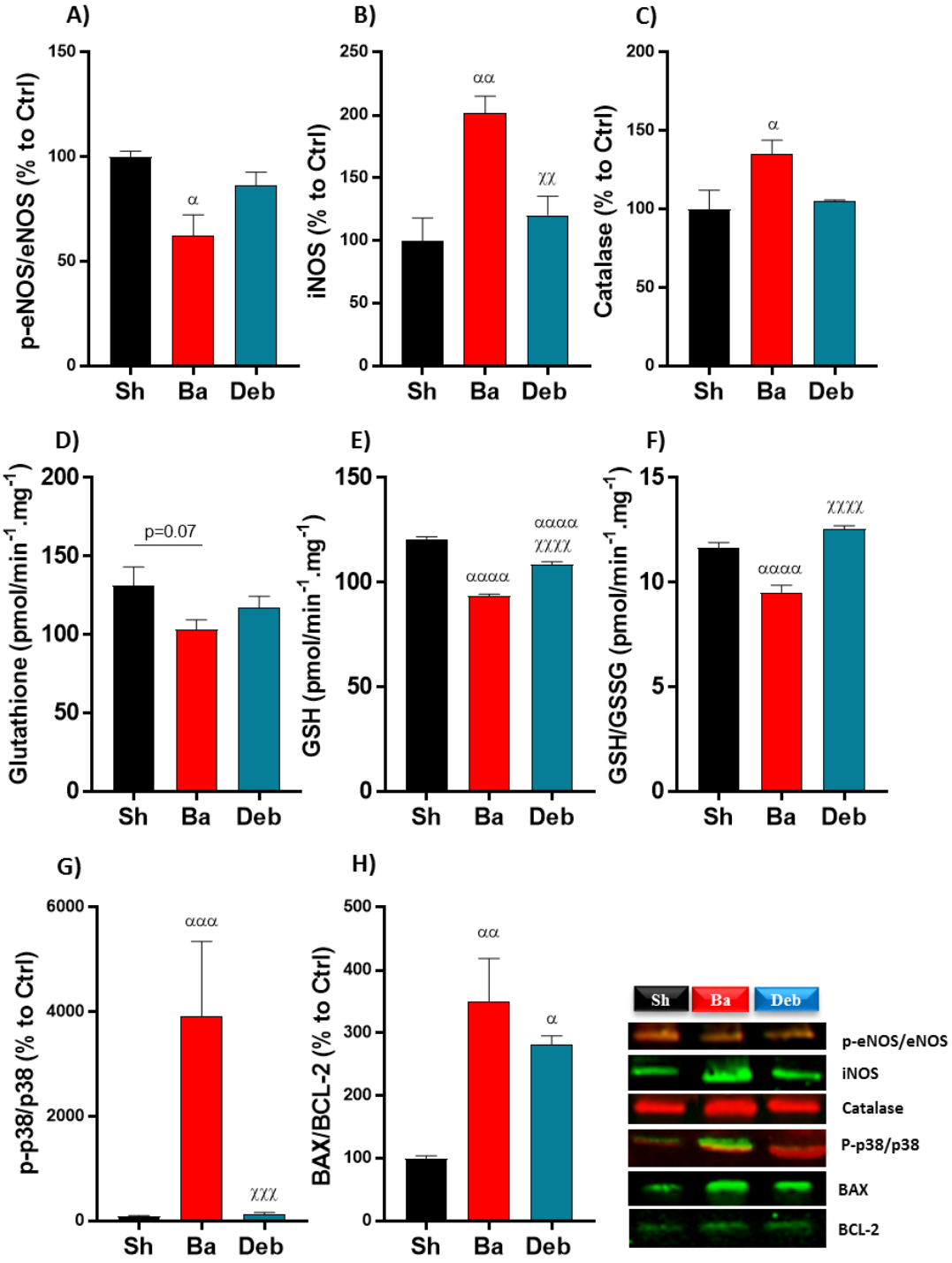

Figure 6- Effect of pressure overload on nitric oxide, antioxidant enzymes, oxidative stress and apoptosis. Western blot relative quantification of: ***A)*** ratio of phosphorylated to total endothelial nitric oxide synthase; ***B)*** ratio of phosphorylated to total inducible nitric oxide synthase; ***C)*** catalase. **Enzymatic determination of*: D)*** Total glutathione; ***E)*** reduced glutathione (GSH); ***F)*** ratio of reduced to oxidized glutathione; ***G)*** ratio of phosphorylated to total p38; ***H)*** ratio of apoptotic Bax to antiapoptotic Bcl-2**.** Representative western blot lanes, phospho antibodies are in green, total antibodies are in red. Values are mean ± SEM. One Way-Anova. ***Ba/Deb vs Sh*****:** α, $p<0.05$; αα, $p< 0.01$; ααα, $p<0.001$; αααα, $p<0.0001$; ***Deb vs Ba:*** χχ, $p<0.01$, χχχ, $p< 0.001$.

g) Metabolic enzymes

In order to evaluate the myocardial energetic metabolic profile, gene expression of some transporters involved in FA and glucose metabolism were analysed by PCR. The improvement of glucose transport in banding animals was proved once PDK4 remains normal (Sh=1.00±0.08; Ba=1.03±0.12; p=0.99, **Figure 7A**) and both GLUT1 and GLUT4 increased significantly (GLUT1: Sh=1.00±0.01; Ba=1.73±0.18; p=0.018 and GLUT4: Sh=1.00±0.04; Ba=1.70.6±0.17; p=0.01, **Figures 7B and C**). In addition, the FA metabolism was unchanged in banding animals since CPT1 was unaffected (Sh=1.00±0.01; Ba=1.21±0.03 p=0.7, **Figure 7D**).

In debanding animals a metabolic shift was observed since PDK4 showed a trend to be up-regulated (Sh=1.00±0.08; Ba=1.03±0.12; Deb=1.89±0.39; Sh vs Deb p=0.10; Ba vs Deb p=0.07, **Figure 7A**). Regarding the glucose transporters, in debanding group we observed a reduction in GLUT1 but not in GLUT4 (GLUT1, Sh=1.00±0.01; Ba=1.73±0.19; Deb=1.35±0.17; Sh vs Deb p=0.20; Ba vs Deb p=0.22; GLUT4, Sh=1.00±0.04; Ba=1.70±0.17; Deb=1.67±0.04; Sh vs Deb p=0.02; Ba vs Deb p=0.99, **Figures 7B and C**). In addition, after afterload alleviation, CPT1expression increased when compared to sham (Sh=1.00±0.01; Ba=1.21±0.03; Deb=1.73±0.24; p=0.04, **Figure 7D**).

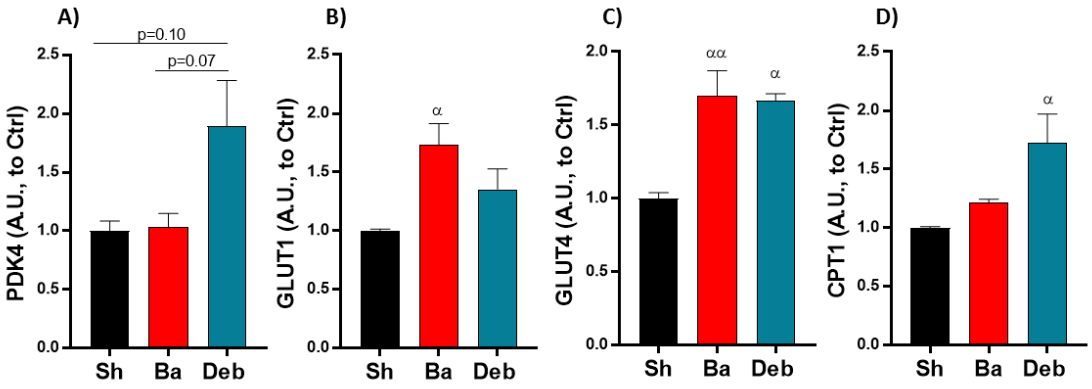

Figure 7- Effect of pressure overload on LV metabolism. Expression of *A)* pyruvate dehydrogenase kinase isoform 4 (PDK4); ***B)*** glucose transporter 1 (GLUT1); ***C)*** glucose transporter 4 (GLUT4); ***D)*** carnitine palmitoyltransferase I (CPT1). One Way-Anova. ***Ba/Deb vs Sh*****:** α, p<0.05; αα, p< 0.01.

h) Mitochondrial biogenesis

To evaluate the mitochondrial structure and morphology in myocardium, electron microscopy and Western Blot were performed. Despite similar number of mitochondria among groups (**Figure 8A**), in banding rats their average area decreased significantly (Sh=49701±2897;

Ba=37524±608, p<0.0001, **Figure 8B**) and mitochondria became more flattened (Sh=0.785±0.005; Ba=0.763±0.005, p=0.04, **Figure 8C**). Concerning mitochondrial dynamics, in banding rats we denoted a trend for PGC-1α upregulation (Sh=100±24; Ba=199±31; p=0.08, **Figure 8D**) and a significant downregulation of MFN1 and MFN2 (MFN1, Sh=100±9; Ba=42±5, p=0.0002; MFN2, Sh=100±1; Ba=59±9; p=0.03, **Figures 8E and F**). Altogether these results suggest an increase of mitochondrial biogenesis and a shift in the balance of dynamics regulation, favouring fission. Curiously, debanding group did not revert mitochondrial alterations (mitochondrial eccentricity, Sh=0.785±0.005; Deb=0.760±0.005, p=0.03; PGC-1α, Sh=100±24; Deb=217±31, p=0.05; MFN1, Sh=100±9; Deb=55±11, p=0.006), except for MFN2, which increased to values similar to those of Sh group (Sh=100±1; Deb=83±1; p=0.35). Concerning the complexes of electron chain transport (ECT) we denoted that, when compared to sham complex I showed a trend to increase in banding group, however complex III and IV decreased significantly (Complex I, Sh=100±4; Ba=131±6, p=0.10; Complex III, Sh=100±12; Ba=63±7, p=0.03; Complex IV, Sh=100±10; Ba=61±5; p=0.004, **Figures 8H, J and K**). Regarding the debanding group we denoted that while complex I increased significantly, complexes III and IV reversed in the formed (Sh=100±12; Ba=63±7; Deb=101±8; Sh *vs* Deb, p= 0.99; Deb *vs* Ba, p= 0.03) but not in the latter. (Sh=100±10; Ba=61±5; Deb=70±8; Sh *vs* Deb, p= 0.06; Deb *vs* Ba, p= 0.68). Moreover, no changes were observed for complex II and V (**Figures I and L**).

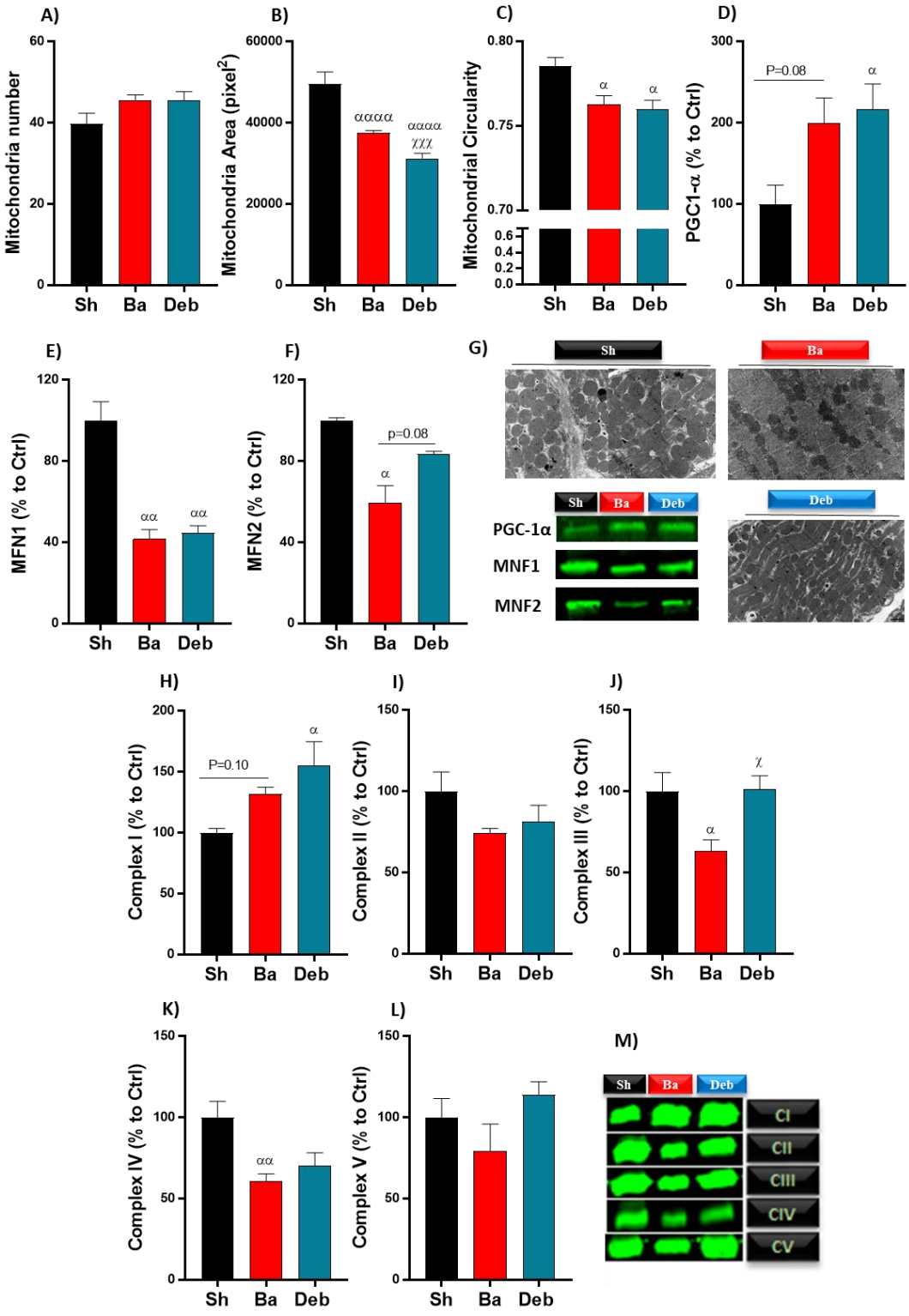

Figure 8- Effect of pressure overload on mitochondrial morphology and biogenesis. Electron microscopy: *A)* mitochondrial number; ***B)*** mitochondrial area; ***C)*** mitochondrial eccentricity; ***D)*** peroxisome proliferator-activated receptor gamma coactivator 1-alpha (PGC-1α); ***E)*** Mitofusin-1 (MFN1); ***F)*** Mitofusin-2 (MFN2); ***G)*** representative images. **Western Blot relative protein quantification of mitochondrial oxidative phosphorylation complexes: *H)*** complex I; ***I)*** complex II; ***J)*** complex III; ***K)*** complex IV; ***L)*** complex V; ***M)*** representative images. Values are mean ± SEM. One Way-Anova: ***Ba/Deb vs Sh:*** *α, p<0.05; αα, p< 0.01; αααα, p<0.0001;* ***Deb vs Ba:*** *χ, p<0.05; χχχ, p< 0.001.*

i) Mitochondrial function

i. Mitochondrial oxygen consumption assays

Since metabolism also depends to mitochondrial function we decided to performed mitochondrial respiration studies by evaluating oxygen consumption in complex I and II of the ECT. Concerning respiratory state 2, we did not observe any difference imposed by banding in complex I or complex II (**Figure 9A**). After ADP addition we denoted a significant increase of respiration rate in banding relative to sham group in complex I and complex II (complex I, Sh=33.42±2.17; Ba=48.9±4.6, p=0.017; complex II, Sh=48.9±2.6; Ba=66.8±1.6, p<0.001, **Figure 9B**). After ADP phosphorylation or state 4, in complex I the mitochondria from banding group continued to consume more oxygen than sham (Sh=7.18±0.31; Ba=9.48±0.49, p=0.007), however, these values are similar to those in state 2 complex I (**Figure 9C**). Despite the increase of oxygen consumption during ADP phosphorylation, mitochondria from banding do not spend more oxygen to phosphorylate the same amount of ADP (**Figure 9D**), denoting that these mitochondria are more efficient and are probably faster in state 3. In the debanding group we observed that, in complex II state 2, mitochondria respiration recovered (Ba=24.0±0.1; Deb=17.6±1.2, p=0.007, **Figure 9A**). In state 3 both complex I and II showed a reduction in oxygen consumption in debanding (complex I, Ba=48.9±4.6; Deb=35.6±4.4, p=0.05; complex II, Ba=66.8±1.6; Deb=49.9±2.0, p<0.001, **Figure 9B**). In state 4 the reduction of oxygen consumption in debanding occurred in both complexes, but in complex I showed a total recovery (complex I, Ba=9.5±0.5; Deb=7.4±0.7, p=0.03; complex II, Ba=27.9±1.7; Deb=23.2±1.1, p=0.17, **Figure 9C**). Despite the total recovery of mitochondrial oxygen consumption observed in debanding group, the efficiency of ADP phosphorylation seems decreased, since the ratio ADP/O in complex I showed a trend to decrease in this group (Sh= 4.3±0.1; Ba=4.5±0.3; Deb=3.4±0.3, Sh vs Deb p=0.18, Ba vs Deb p=0.058, **Figure 9D**).

Higher RCR's, as observed in the banding group, implies that the mitochondria have a higher capacity for substrate oxidation, ATP turnover and a low proton leak (complex I, Sh=4.5±0.3 Ba=5.2±0.2, p=0.09; complex II, Sh=2.0±0.1; Ba=2.4±0.1, p=0.05, **Figure 9E**). Together these results highlight the good performance of mitochondria in the banding group.

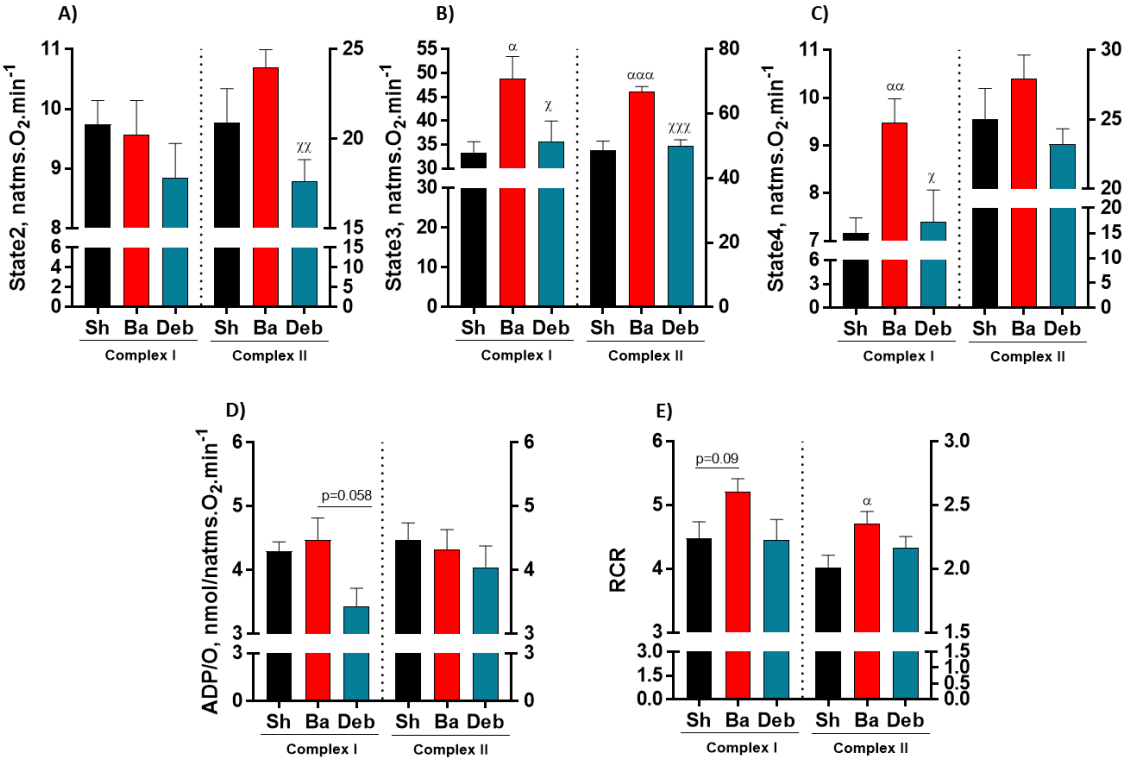

Figure 9- Effect of pressure overload on mitochondrial respiration. Complex I and II respiration at *A)* state 2; ***B)*** state 3; ***C)*** state 4; ***D)*** ratio of ADP phosphorylated to oxygen consumption; ***E)*** respiratory control ratio. Values are mean ± SEM. One Way-Anova. ***Ba/Deb vs Sh:*** *α, p<0.05; αα, p< 0.01; ααα, p<0.001****; Ba vs Deb:*** *χ, p<0.05; χχ, p<0.01, χχχ, p< 0.001.*

ii. Mitochondrial transmembrane electrical potential assays and uncoupling

Mitochondrial membrane potential is critical for maintaining the physiological function of the respiratory chain, i.e., to generate ATP. In banding animals we denoted a significant increase of maximum potential at both complexes (complex I, Sh=168.1±0.7; Ba=170.9±0.6, p=0.01; complex II, Sh=172.6±0.6; Ba=175.7±0.8, p=0.03, **Figure 10A**). The same pattern was observed in repolarization (complex I, Sh=169.2±0.7; Ba=172±0.6, p=0.03; complex II, Sh=175.6±0.6; Ba=178.3±0.8, p= 0.04, **Figure 10C**). In debanding rats we observed a normalization of maximum potential in both complexes (complex I, Ba=170.9±0.6; Deb=167.5±0.7, p=0.007; complex II, Ba=175.7±0.8; Deb=171.3±1.04, p=0.003, **Figure 10A**). The same pattern was observed in repolarization (complex I, Ba=172±0.6; Deb=168.3±0.9; p=0.008; complex II, Ba=178.3±0.7645; Deb=172.9±0.9, p=0.0002, **Figure 10C**). Curiously, in complex II the values of repolarization observed in debanding showed a trend to decrease beyond the sham values (Sh=175.6 ± 0.6434; Deb=172.9±0.9, p=0.06, **Figure 10C**). The mitochondrial membrane potential during depolarization did not show any significant difference between the groups (**Figure 10B**).

The physiological functions of UCP include lowering mitochondrial membrane potential, dissipating metabolic energy in the form of heat and reducing oxidative stress. Since we observed an increase of oxidative stress and alterations in membrane potential in banding animals, we decided to evaluate UCP-1. This uncoupling protein increased in banding animals when compared to sham animals (Sh=100±17; Ba=178±8; p=0.04, **Figure 10D**), denoting an increased heat production. The removal of the aortic constriction reduced UCP-1 to values similar to those of sham values, but not sufficient to be different from banding group (Sh=100±17; Ba=178 ± 8; Deb=142±30; Sh *vs* Deb p=0.37; Ba *vs* Deb p=0.32, **Figure 10D**).

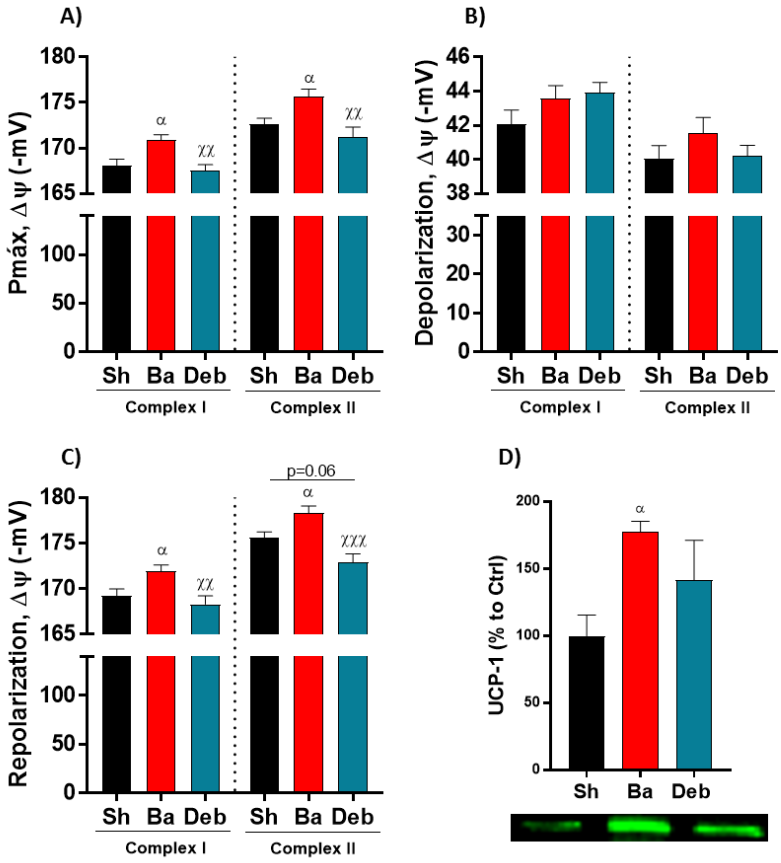

Figure 10- Effect of pressure overload on mitochondria membrane potential. ***A)*** maximum membrane potential in complex I and in complex II; ***B)***; membrane potential during depolarization in complex I and in complex II; ***C)*** membrane potential during repolarization in complex I and in complex II; ***D)*** relative quantification of uncoupling protein 1. Values are mean ± SEM. One Way-Anova. ***Ba/Deb vs Sh:*** *α, p<0.05;* ***Deb vs Ba:*** *χχ, p<0.01, χχχ, p< 0.001.*

j) Skeletal muscle

i. Aerobic capacity and effort training

Exercise incapacity is a hallmark of HFpEF, so we evaluated the aerobic capacity in our rats. In the banding animals we observed a reduction of all the parameters evaluated, namely, running time (Sh=13.16±0.55; Ba=11.13±0.37, p=0.02, **Figure 11A**), VO_2max (Sh=33.26±1.04; Ba=29.17±0.70, p=0.01, **Figure 11B**), VCO_2max (Sh=28.7±0.9; Ba=25.24±0.59, p=0.02, **Figure 11C**), and EE (Sh=233.3±7.1; Ba=206.1±4.9, p=0.02, **Figure 11D**), highlight the reduced capacity to exercise present in these animals. In the debanding group we showed a total recovery of running time denoting a better exercise performance in these animals (Ba=11.13±0.37; Deb=13.32±0.53, p=0.01, **Figure 11A**). Additionally, debanding rats partially recovered VO_2max, VCO_2max and EE (VO_2max Ba=29.17±0.70; Deb=31.3±0.8, p=0.4307; VCO_2max Ba=25.24±0.59; Deb=27.99±0.77, p=0.07; EE Ba=206.1±4.9; Deb=220.5±5.4, p=0.33, **Figures 11B, C and D**).

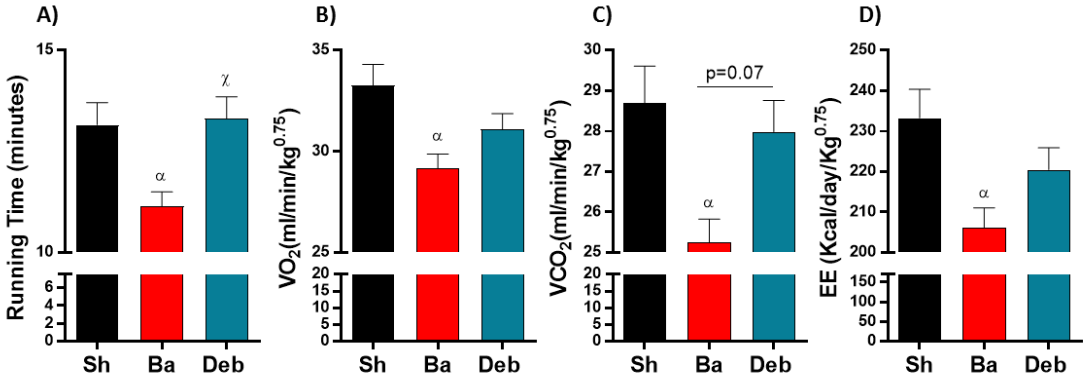

Figure 11-Effect of pressure overload on aerobic capacity. ***A)*** running time; ***B)*** maximum rate of oxygen consumption ***C)*** maximum CO2 elimination ***D)*** energy expenditure. Values are mean ± SE, One-way anova. ***Ba/Deb vs Sh:*** *α, p<0.05;* ***Deb vs Ba:*** *χ, p<0.05.*

ii. Myocytes atrophy and fibrosis

In the skeletal muscle, we observed an atrophy of myocytes, as assessed by its area that decreased significantly (Sh=2448±198; Ba=1731±100, p=0.04, **Figures 12A and B**). Skeletal atrophy recovered after removing aortic constriction (Sh=2448±198; Ba=1731±100; Deb=2039±189, Sh vs Deb p= 0.42, Ba vs Deb p=0.31, **Figures 12A and B**). In the same muscle, the skeletal myocytes fibrosis increased in banding (Sh=2.04±0.17; Ba=2.89±0.27, p=0.03, **Figures 12C and D**). The debanding procedure induced a reduction of skeletal muscle fibrosis that normalized in the debanded group (Sh=2.04±0.17; Ba=2.89±0.27; Deb=2.42±0.36, Sh *vs* Deb p=0.47, Deb *vs* Ba p=0.67, **Figures 12C and D**).

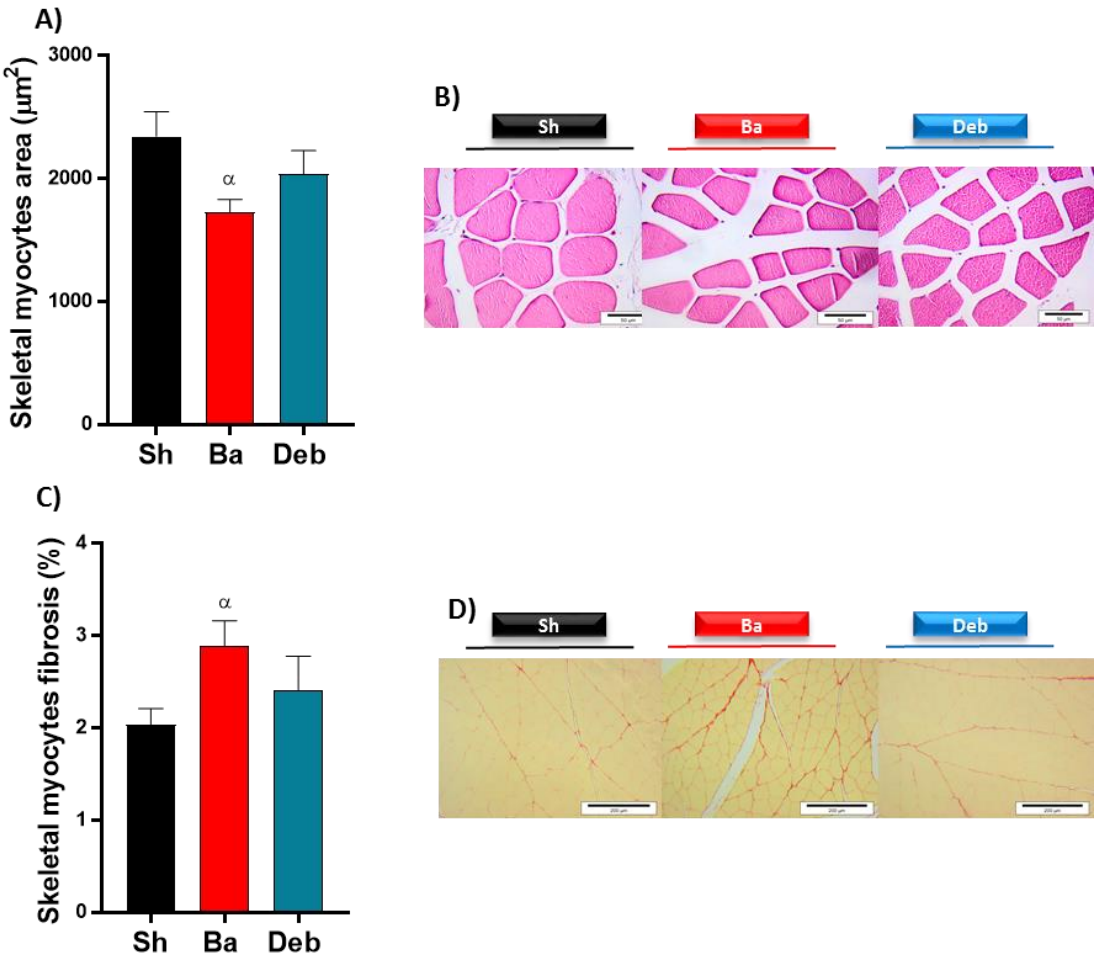

Figure 12-Effect of pressure overload on skeletal myocyte area and fibrosis. ***A)*** myocyte area, ***B)*** representative images of hematoxylin-eosin staining, ***C)*** myocyte fibrosis, ***D)*** representative images of picrosirius *red* staining . Values are mean ± SEM. One-Way anova. ***Ba/Deb vs Sh****: α, p<0.05*.

iii. Metabolic enzymes

In order to evaluate the energetic metabolic profile in skeletal muscle, expression of some transporters involved in metabolism of FA and glucose were analysed by PCR. Curiously in the banding group we observed an increase of both glucose and FA metabolism (PDK4, Sh=1.00±0.04; Ba=2.27±0.13, p=0.001; GLUT1 Sh=1.00±0.07; Ba=1.83±0.28, p=0.009 and GLUT4 Sh=1.00±0.05; Ba=1.30±0.01, p=0.011; CPT1 Sh=1.00±0.03; Ba=1.46±0.08; p=0.01, **Figures 13A, B, C and D**). Upon overload relieved, the expression of PDK4 and CPT1 increased further compared to banding (PDK4, Ba=2.27±0.13, Deb=3.26±0.31; p=0.008; CPT1, Ba=1.46±0.08; Deb=1.79±0.14, p=0.05) (**Figures 13A and D**), while GLUT1 and GLUT4 normalized (GLUT1, Ba=1.83±0.28, Deb=0.73±0.02, p<0.001; GLUT4, Ba=1.30±0.01, Deb=1.09±0.09, p=0.08, **Figures 13B and C**).

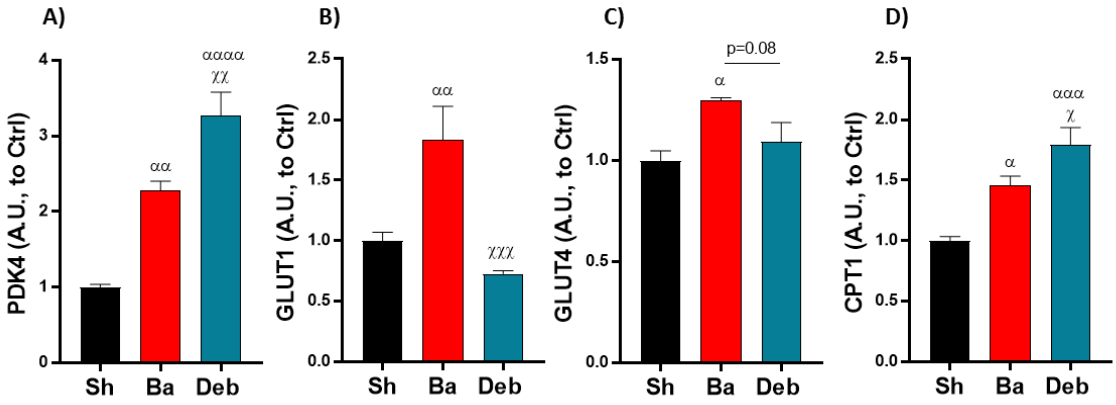

Figure 13- Effect of pressure overload on skeletal muscle metabolism. ***A)*** pyruvate dehydrogenase kinase isoform 4, ***B)*** Glucose transporter 1, ***C)*** Glucose transporter 4, ***D)*** Carnitine palmitoyltransferase I**.** Values are mean ± SE, One-way anova. ***Ba/Deb*** *vs Sh: α, p<0.05; αα, p< 0.01; ααα, p<0.001; αααα, p<0, 0001;* ***Deb vs Ba****: χ, p<0.05; χχ, p<0.01, χχχ, p< 0.001.*

DISCUSSION

In this study, we show that we have successfully implemented an animal model that mimics the phenotype of left ventricular concentric remodelling and reverse remodelling. This animal model presents diastolic dysfunction and evidences all signs typical of HFpEF, such as concentric hypertrophy, increased cardiomyocyte stiffness and alterations in myofilaments calcium handling. Moreover, in banding animals the structural and metabolic changes at skeletal muscle level could be behind to exercise intolerance. When the afterload was alleviated, we observed a normalization of ventricular mass but cardiomyocyte hypertrophy remained higher than sham. Moreover, in debanding rats we observed a better filling pattern during diastole that could be due to, at least in part to the partial reduction of: oxidative stress; NO bioavailability; titin phosphorylation; cardiomyocyte stiffness and increase of calcium reuptake to sarcoplasmic reticulum. However, myocardial fibrosis and apoptosis remained upper. The better cardiac performance in debanding group followed the improvement of myofilaments response to calcium but cardiac shortening and myocyte force redevelopment remained reduced.

In the hypertrophic heart, was observed changes in mitochondrial expression that suggest an increase of biogenesis and fission without changes in mitochondria number however, we denoted an improvement of mitochondria functionality followed by the augment of glucose transporters, suggesting a metabolic shift. When afterload was relieved, the normalization of mitochondrial function but not morphology occurred and was followed by the augment of lipid transporters and oxidation, as well as an augment of complex I expression.

The over-expression of uncoupling proteins and the downregulation of complexes III and IV could represent an attempt to reduce oxidative stress but, after debanding we only observed a partial recovery of UCP-1 and complex IV.

After debanding the running time reached the control values, but the aerobic capacity and the skeletal muscle abnormalities only recovered partially. Metabolically, while glucose transporters normalized, fatty acid transporters and utilization increased.

As previously described, after a pressure overload stimulus as occurs in HFpEF, LV hypertrophy installs, ventricular walls thicken and cavities decrease, which leads to an increase in LV mass [107]. Similar to what we have reported, a precious study on aortic constriction-induced hypertrophy described raised levels of AKT, mTOR, and GSK3β phosphorylation [108]. The increased phosphorylation of these proteins represent steps of a signalling pathway that culminates in increased hypertrophy, since AKT activation blocks the anti-hypertrophic activity of GSK3β while promoting mTOR activity [109]. Debanding induced ventricular RR, but only partially, as observed in posterior walls thickness and LV mass. Moreover, and as previously reported [31, 92]

the cardiomyocytes remains hypertrophic, which could contributes to GSK3β hyperphosphorylation.

The presence of diastolic dysfunction was evident in banding animals by the decreased E/A ratio as well as the increase of E/E´ and left atrium area [107]. These filling alterations occurs concomitantly with the augment of cardiomyocytes' passive tension, that could result from changes at myofilamentary proteins such titin or, at higher sarcomere lengths from ECM stiffness [110]. In the present study we observed hyperphosphorylation of titin and PEVK segment. The same results were reported in a similar study as contributors to the increase of passive tension [110], however, titin hypophosphorylation is frequently associated to myocardial stiffness in HFpEF [111]. The removal of constriction induced a partial reduction on titin phosphorylation and a decreased on cardiomyocyte passive tension. Concerning ECM alterations, we denoted an increase of fibrosis deposition on myocardial tissue accomplished by the augment of gene expression of TGF-β and procollagen I and III respectively, which are in agreement with previous studies [112]. TGF-β can promote collagen deposition by inducing the synthesis of collagen I and III and by inhibiting its degradation. Thus TGF-β promotes myocardial stiffness and dysfunction [74, 75]. After afterload relief, myocardial fibrosis persisted but we observed a reduction of TGF-β and a total reversion on procollagen I and III. Curiously, similar results were obtained in humans after LVAD implantation [113], translating the earlier molecular rather than the histological changes. Pulmonary congestion in banding animals evidenced by increased lung weight was observed. Right atrial enlargement and a decreased of TAPSE also reveals right dysfunction in these animals as supported by previous studies [114].

Despite a small decrease of myocardial performance in banding animals, as assessed by the decrease of TEI index and fractional shortening (FS), cardiac function was maintained since EF is preserved, thus mimicking HFpEF-phenotype [107]. The increase of intracellular calcium coupled to a reduction of the activity and/or expression of SERCA-2a and NCX have been documented in HFpEF, congestive HF, and was also observed by us in banding rats [115, 116]. As a consequence of calcium handling dysregulation and the resultant increase of intracellular calcium, the myofilaments active force, calcium sensitivity and nHill increases, while Ktr decreases, as previously described by our group [112]. Moreover, these alterations also impair calcium reuptake to SR and thus relaxation. When aortic constriction was removed we observed an improvement of calcium handling proteins denoting a reduction of cytoplasmic calcium and a better relaxation, however, we did not detect any improvement on Ktr.

NO is an important mediator of cardiac function whose levels are downregulated in HF compromising its beneficial actions [117]. Additionally to NO levels, the importance of NOS uncoupling in hypertrophic heart disease has been previously highlighted since NOS re-coupling by

exogenous BH4 ameliorates pre-existing advanced cardiac hypertrophy and fibrosis [118]. In macrophages, iNOS expression and arginase increase concomitantly, reducing the availability of arginine to iNOS. With substrate limitation, iNOS may become uncoupled and produce ROS [119]. In cardiac tissue, AKT, mitogen-activated protein kinase p42/44 or extracellular signal-regulated kinase (ERK1/2) are involved in regulation of iNOS activity or expression. In agreement with our data, an increase of iNOS expression in cardiac hypertrophy after aortic banding has previously been reported. Moreover, the inhibition of iNOS not only reduced LV hypertrophy, AKT and mTOR activation, pulmonary congestion or LV fibrosis but also oxidative stress [120]. In HFpEF, increased ROS promote oxidative stress that induce mitochondrial damage and cardiac dysfunction [41]. In fact, in the myocardium from banding rats we denoted an upregulation of catalase and a reduction of glutathione, denoting an increase of oxidative stress that was attenuated after debanding. Similar results had been previously described after LVAD implantation [49].

In HF, the downregulation of eNOS contributes to disease progression and when eNOS becomes overexpressed, an attenuation of LV remodelling induced by aortic constriction as well as p38 activation [121] is observed. In our work, the decrease of eNOS and the increase of p38 activation in banding rats could be involved on cardiac remodelling. Indeed, at cardiac level, p38 activation can promote hypertrophy, fibrosis, apoptosis and thus cardiac dysfunction. In aortic banding rats we observed an increase of apoptosis that was also described for spontaneously hypertensive rats (SHR) or isoproterenol-treated rats myocardium [122]. After aortic constriction relief, the reduction of iNOS and increase of eNOS occurred simultaneously to the normalization of antioxidant enzymes and p38, denoting a reduction of oxidative stress. These results are not surprising since endogenous NO increase after LVAD implantation [49]. However, after debanding while apoptosis markers remains higher, p38 activation reached the control values, meaning that other proteins than p38 underlie apoptosis activation [123, 124]. Despite the increase of apoptosis in banding rats, its cardiac mass is higher than in sham. This can occur if apoptosis affects predominantly non-myocyte cell, as described in cardiac hypertrophy [125].

It is known that the aortic banding-induced hypertrophy is characterized by functional and structural mitochondrial alterations, however the scarcity of results are still contradictory. Similar to that was described for ischemic HF, our results evidenced structural mitochondrial alterations induced by banding, that suggest upregulation of mitochondrial fission [126]. Moreover, the reduction of proteins involved in fusion processes (MFN 1 and MFN 2) are associated with an augment of mitochondrial fragmentation [127]. Curiously, in debanding, the mitochondria are still smaller than sham, despite the augment of MFN 2. This finding could be explained by its important role in calcium regulation since MFN 2 is crucial to tether SR to mitochondria [128]. In banding rats, a reduction in SERCA-2a, NCX as well as PLB activation was observed, denoting, as

previously reported an increase in cytosolic Ca^{2+} [129] that was restored after debanding. Thus, the role of MFN 2 in mitochondrial Ca^{2+} uptake becomes futile in banding animals. However, when a reduction of the cytosolic Ca^{2+} levels occurred, an increase of MFN 2 was observed probably to re-establish the mitochondrial levels of calcium. Despite the increase of PGC-1α and the presence of small mitochondria, the mitochondrial number remained unchanged in banding animals as had previously been described in a HF model induced by aortic constriction [48]. However, it should be noted that some studies performed in chronic pressure overload did not report an increased PGC-1α [48], but this may be due to severity of HF, since at the time of sacrifice, the systolic function of these animals was already deteriorated. Additionally, the increase in mitochondrial biogenesis in hypertrophy , could delay cardiac decompensation induced by pressure overload [130]. However, the unchanged number of mitochondria is not compatible with the probable mitochondrial fission process nor with the observed increased PGC-1α expression. A potential explanation for these findings could be the high apoptosis markers in these animals, evidenced by the elevated p38 activation and Bax/Bcl-2 ratio, which seems to prevail over mitochondrial biogenesis.

Contrary to our results, in both aortic constriction and ischemic HF-animal models, a decrease in state 3 respiration rate without state 4 alteration was reported [48, 126]. Moreover, a decrease in the expression and activity of complex I and V without alterations in the activity of complexes II and IV was also observed in other HF-animals models [126, 131]. However, as cardiac hypertrophy impairs the relationship between ATP demand and production, mitochondrial bioenergetics must keep up with the cardiac mass increase [130]. Thus, the increase in respiration observed in banding rats could represent an attempt to overcome the energetic load imposed by aortic constriction. Reinforcing our data, an increase in mitochondrial respiration had previously been described in non-failing hypertrophic human hearts [132]. Additionally, in rabbits and rats submitted to aortic constriction was reported an increase of respiratory capacity of isolated mitochondria and an upregulation of oxidative phosphorylation rates during the early stage of hypertrophy followed by a decline, coinciding with the drop in contractility and EF, indicative of HF progression [133, 134]. Similar to us, these results suggests a compensatory increase in mitochondrial respiration and oxidative phosphorylation during early cardiac hypertrophy. Curiously, we observed that ADP/O ratio was unchanged in banding which probably denotes a reduction in phosphorylation time. Complex I is the largest enzyme and plays critical roles both in transferring electrons from reduced NADH to Coenzyme Q and in maintaining the proton electrochemical gradient across the inner mitochondrial membrane. In our study, we observed an increase of complex I in banding rats that could be a consequence of the metabolic shift towards glucose. The metabolic substrate in hypertrophic hearts shifts toward glucose during stress conditions, such as ischemia and pathological hypertrophy [135]. Indeed, the unchanged expression

of FAT/CD36, CPT1 or CPT2 or an increase of GLUT4 and lactate dehydrogenase is well documented [24]. This metabolic shift toward glucose utilization can compromise the energetic state of the myocardium, because the net yield of ATP production per mole of FA oxidation is greater than the one of glucose. However, glucose has less oxygen costs, and thus this shift could represent a compensatory mechanism to balance the potential reduction in oxygen availability. In the present work, while glucose transporters were upregulated, both the rate-limiting enzyme in β-oxidation of FA (CPT1) and the enzyme responsible for the phosphorylation and inhibition of the pyruvate dehydrogenase (PDH) complex, PDK4, remain normal. This possibly means that glucose oxidation and glycolysis are uncoupled, as previously reported by others [136]. After overload relief, we observed an upregulation of PDK4 and CPT1, while GLUT1 reversed and GLUT4 remained higher. In myocardium, overexpression of PDK4, is sufficient to cause a decrease in glucose catabolism and an increase in FA oxidation [137]. Indeed, our results are in agreement with previous work reporting an improvement of FA oxidation after LVAD implantation [96].

Despite the increase in complex I, complex III and IV did not follow this trend and were downregulated in banding rats. Since complex I, III, and IV are the main ROS producers, the downregulation of both complexes III and IV could represent an attempt to control ROS. However, other possible explanation can be the reversible inhibition of cytochrome *c* oxidase by NO as an attempt to regulate tissue oxygen gradients [138]. Despite the reported inhibition of mitochondrial respiration by NO, in hypertrophied hearts submitted to aortic constriction, 52% complex IV inhibition was required to inhibit mitochondrial respiration half maximally [63]. Thus, the increase in mitochondrial respiration can occur simultaneously to complex IV inhibition. The decrease levels of complexes III and IV as well as UCP upregulation could decrease the proton gradient across the membrane and could represent a mechanism to stabilize membrane potential that was higher in banding rats. The mitochondrial proton circuit is essential to the multiple physiological functions of mitochondria [139],[140], and is largely completed by the proton leak, which may serve an important purpose in limiting proton-motive force (pmf), to prevent dielectric breakdown of the membrane and restrict leakage of single electrons from the electron transport chain to form superoxide [139]. Thus, elevated levels of mitochondrial membrane potential ($\Delta\Psi_m$) can stimulate mitochondrial ROS production [141]. In cardiomyocyte hypertrophy induced by norepinephrine the reduction on ATP levels was associated to the reduction on mitochondrial membrane potential (Ψ_m) [142], however, in right ventricle hypertrophy, phenylephrine caused a significant increase in mitochondrial membrane potential [143]. In aortic banding rats, the increase of UCP-1 seems to delay the progression to HF [144]. After aortic debanding the functional alterations observed in mitochondria were restored, however concerned mitochondrial morphology, the same was not true since the biogenesis and fission mechanism remained augmented. In banding rats, and according

with previous studies, a metabolic shift favouring glucose oxidation was observed [24]. However, after pressure unloading the lipid oxidation also increased, which is in agreement previous studies in rats and in humans that showed an improvement of energetic metabolism in myocardium after debanding or LVAD implantation [94, 96]. Interestingly these alterations in myocardial metabolism did not result in the reduction of complex I or increase in complex IV expression, despite the normalization of mitochondrial respiration and membrane potential, which probably could denote some functional changes at the complexes levels.

Exercise intolerance is a hallmark of HFpEF that usually correspond to the peak of consumed O_2 during the maximal effort [79, 80]. Not surprisingly, we observed a reduction of aerobic capacity in our banding rats that was completed reversed after afterload alleviation. Both cardiac and peripheral factors are pointed out to the main contributors to exercise incapacity in HFpEF patients. Among these factors, an inadequate extraction/utilization of O_2 or intrinsic skeletal muscle dysfunction characterized by the reduction of the ratio capillary/fibre and fibre atrophy seems to be more prevalent. Indeed, we observed that the animals that presented a reduction on aerobic capacity showed myocyte atrophy and fibrosis which is in accordance with previous reported outcomes in skeletal biopsies from HFpEF patients [87]. Some evidence concerning the imbalance between protein synthesis and degradation or even the involvement of alterations in the ubiquitin-proteasome system and the activation of apoptosis pathway could be responsible for the myocyte atrophy observed in skeletal muscle [145]. In our banding rats we denoted an overexpression of glucose transporters however, glucose oxidation did not increase since the pyruvate dehydrogenase complex was strongly inhibited by PDK4. This could result from lower oxygen bioavailability that promotes the mobilization of pyruvate to other metabolic pathways, or even mitochondrial dysfunction that compromises glucose and FA oxidation. In fact, a reduction of mitochondrial content, oxygen consumption and lower RCR were reported in skeletal muscle biopsies from HFpEF patients [90, 92], as well as an increase of diacylglycerol and ceramide content [94]. However, our animals with chronic pressure overload showed an increase of CPT1, but this increase could only represent a compensatory mechanism. When afterload was alleviated the reduction on glucose transporters was accomplished by the increase of PDK4 and CPT1, denoting a metabolic shift that promotes FA oxidation. Indeed, the aerobic intolerance in banding animals could be, at least in part, a consequence of metabolic shift and therefore the myocyte alteration and stiffness observed in skeletal muscle.

CONCLUSION

This work show that the banding/debanding in Wistar Rats is a good animal model to study the mechanism behind the cardiac remodelling and reverse remodelling in HFpEF.

Beyond concentric hypertrophy, diastolic dysfunction and calcium dysregulation, we founded that mitochondria and oxidative stress are also involved in the compensatory adaptation of myocardium to afterload. Moreover, during cardiac adaptation metabolic flexibility occurred, probably as a compensatory mechanism, since glucose oxidation can save more oxygen than FA.

After debanding, the normalization of cardiac function was not followed by the reversion of cardiac structure, myocardial fibrosis and apoptosis. Additionally, mitochondria are still smaller than sham, and was observed an augment of FA transporters and inhibition of glucose oxidation.

Additionally to cardiac abnormalities, the alterations founded in skeletal muscle could be behind the exercise intolerance observed in HFpEF, reinforcing the idea this syndrome is more than a heart disease.

BIBLIOGRAPHY

1. Fukuta, H. and W.C. Little, *The cardiac cycle and the physiologic basis of left ventricular contraction, ejection, relaxation, and filling.* Heart Fail Clin, 2008. **4**(1): p. 1-11.
2. Gomes, M.C., A. Ferreira, and P. Bettencourt, *[Physiopathology of heart failure].* Rev Port Cardiol, 2004. **23 Suppl 2**: p. Ii7-23.
3. Stanley, W.C., F.A. Recchia, and G.D. Lopaschuk, *Myocardial substrate metabolism in the normal and failing heart.* Physiol Rev, 2005. **85**(3): p. 1093-129.
4. Mosterd, A. and A.W. Hoes, *Clinical epidemiology of heart failure.* Heart, 2007. **93**(9): p. 1137-46.
5. Ponikowski, P., A.A. Voors, S.D. Anker, H. Bueno, J.G. Cleland, A.J. Coats, V. Falk, J.R. Gonzalez-Juanatey, V.P. Harjola, E.A. Jankowska, M. Jessup, C. Linde, P. Nihoyannopoulos, J.T. Parissis, B. Pieske, J.P. Riley, G.M. Rosano, L.M. Ruilope, F. Ruschitzka, F.H. Rutten, and P. van der Meer, *2016 ESC Guidelines for the diagnosis and treatment of acute and chronic heart failure: The Task Force for the diagnosis and treatment of acute and chronic heart failure of the European Society of Cardiology (ESC). Developed with the special contribution of the Heart Failure Association (HFA) of the ESC.* Eur J Heart Fail, 2016. **18**(8): p. 891-975.
6. Ferrari, R., M. Bohm, J.G. Cleland, W.J. Paulus, B. Pieske, C. Rapezzi, and L. Tavazzi, *Heart failure with preserved ejection fraction: uncertainties and dilemmas.* Eur J Heart Fail, 2015. **17**(7): p. 665-71.
7. Wambolt, R.B., G.D. Lopaschuk, R.W. Brownsey, and M.F. Allard, *Dichloroacetate improves postischemic function of hypertrophied rat hearts.* J Am Coll Cardiol, 2000. **36**(4): p. 1378-85.
8. Dai, D.F., E.J. Hsieh, T. Chen, L.G. Menendez, N.B. Basisty, L. Tsai, R.P. Beyer, D.A. Crispin, N.J. Shulman, H.H. Szeto, R. Tian, M.J. MacCoss, and P.S. Rabinovitch, *Global proteomics and pathway analysis of pressure-overload-induced heart failure and its attenuation by mitochondrial-targeted peptides.* Circ Heart Fail, 2013. **6**(5): p. 1067-76.
9. Shi, J., W. Dai, S.L. Hale, D.A. Brown, M. Wang, X. Han, and R.A. Kloner, *Bendavia restores mitochondrial energy metabolism gene expression and suppresses cardiac fibrosis in the border zone of the infarcted heart.* Life Sci, 2015. **141**: p. 170-8.
10. Sharma, K. and D.A. Kass, *Heart failure with preserved ejection fraction: mechanisms, clinical features, and therapies.* Circ Res, 2014. **115**(1): p. 79-96.
11. Lam, C.S., E. Donal, E. Kraigher-Krainer, and R.S. Vasan, *Epidemiology and clinical course of heart failure with preserved ejection fraction.* Eur J Heart Fail, 2011. **13**(1): p. 18-28.
12. Borlaug, B.A. and W.J. Paulus, *Heart failure with preserved ejection fraction: pathophysiology, diagnosis, and treatment.* Eur Heart J, 2011. **32**(6): p. 670-9.
13. Divakaruni, A.S. and M.D. Brand, *The regulation and physiology of mitochondrial proton leak.* Physiology (Bethesda), 2011. **26**(3): p. 192-205.
14. Steinberg, B.A., X. Zhao, P.A. Heidenreich, E.D. Peterson, D.L. Bhatt, C.P. Cannon, A.F. Hernandez, and G.C. Fonarow, *Trends in patients hospitalized with heart failure and preserved left ventricular ejection fraction: prevalence, therapies, and outcomes.* Circulation, 2012. **126**(1): p. 65-75.
15. Paulus, W.J. and C. Tschope, *A novel paradigm for heart failure with preserved ejection fraction: comorbidities drive myocardial dysfunction and remodeling through coronary microvascular endothelial inflammation.* J Am Coll Cardiol, 2013. **62**(4): p. 263-71.
16. Huis In 't Veld, A.E., F.S. de Man, A.C. van Rossum, and M.L. Handoko, *How to diagnose heart failure with preserved ejection fraction: the value of invasive stress testing.* Neth Heart J, 2016. **24**(4): p. 244-51.
17. Scheubel, R.J., M. Tostlebe, A. Simm, S. Rohrbach, R. Prondzinsky, F.N. Gellerich, R.E. Silber, and J. Holtz, *Dysfunction of mitochondrial respiratory chain complex I in human failing myocardium is not due to disturbed mitochondrial gene expression.* J Am Coll Cardiol, 2002. **40**(12): p. 2174-81.

18. Decherd, G. and M.B. Visscher, *Energy Metabolism of the Failing Heart.* J Exp Med, 1934. **59**(2): p. 195-9.
19. Doenst, T., T.D. Nguyen, and E.D. Abel, *Cardiac metabolism in heart failure: implications beyond ATP production.* Circ Res, 2013. **113**(6): p. 709-24.
20. Eleid, M.F., R.A. Nishimura, P. Sorajja, and B.A. Borlaug, *Systemic hypertension in low-gradient severe aortic stenosis with preserved ejection fraction.* Circulation, 2013. **128**(12): p. 1349-53.
21. Huss, J.M. and D.P. Kelly, *Mitochondrial energy metabolism in heart failure: a question of balance.* J Clin Invest, 2005. **115**(3): p. 547-55.
22. Akki, A., K. Smith, and A.M. Seymour, *Compensated cardiac hypertrophy is characterised by a decline in palmitate oxidation.* Mol Cell Biochem, 2008. **311**(1-2): p. 215-24.
23. Allard, M.F., B.O. Schonekess, S.L. Henning, D.R. English, and G.D. Lopaschuk, *Contribution of oxidative metabolism and glycolysis to ATP production in hypertrophied hearts.* Am J Physiol, 1994. **267**(2 Pt 2): p. H742-50.
24. Degens, H., K.F. de Brouwer, A.J. Gilde, M. Lindhout, P.H. Willemsen, B.J. Janssen, G.J. van der Vusse, and M. van Bilsen, *Cardiac fatty acid metabolism is preserved in the compensated hypertrophic rat heart.* Basic Res Cardiol, 2006. **101**(1): p. 17-26.
25. Taylor, M., T.R. Wallhaus, T.R. Degrado, D.C. Russell, P. Stanko, R.J. Nickles, and C.K. Stone, *An evaluation of myocardial fatty acid and glucose uptake using PET with [18F]fluoro-6-thia-heptadecanoic acid and [18F]FDG in Patients with Congestive Heart Failure.* J Nucl Med, 2001. **42**(1): p. 55-62.
26. Young, M.E., F.A. Laws, G.W. Goodwin, and H. Taegtmeyer, *Reactivation of peroxisome proliferator-activated receptor alpha is associated with contractile dysfunction in hypertrophied rat heart.* J Biol Chem, 2001. **276**(48): p. 44390-5.
27. Noma, T., A. Nishiyama, K. Mizushige, K. Murakami, T. Tsuji, M. Kohno, M. Rahman, T. Fukui, Y. Abe, and S. Kimura, *Possible role of uncoupling protein in regulation of myocardial energy metabolism in aortic regurgitation model rats.* Faseb j, 2001. **15**(7): p. 1206-8.
28. Stride, N., S. Larsen, M. Hey-Mogensen, K. Sander, J.T. Lund, F. Gustafsson, L. Kober, and F. Dela, *Decreased mitochondrial oxidative phosphorylation capacity in the human heart with left ventricular systolic dysfunction.* Eur J Heart Fail, 2013. **15**(2): p. 150-7.
29. Wambolt, R.B., S.L. Henning, D.R. English, Y. Dyachkova, G.D. Lopaschuk, and M.F. Allard, *Glucose utilization and glycogen turnover are accelerated in hypertrophied rat hearts during severe low-flow ischemia.* J Mol Cell Cardiol, 1999. **31**(3): p. 493-502.
30. Bayeva, M., M. Gheorghiade, and H. Ardehali, *Mitochondria as a therapeutic target in heart failure.* J Am Coll Cardiol, 2013. **61**(6): p. 599-610.
31. Poulsen, S.H., P. Sogaard, J.E. Nielsen-Kudsk, and H. Egeblad, *Recovery of left ventricular systolic longitudinal strain after valve replacement in aortic stenosis and relation to natriuretic peptides.* J Am Soc Echocardiogr, 2007. **20**(7): p. 877-84.
32. Khuchua, Z.A., R. Ventura-Clapier, A.V. Kuznetsov, M.N. Grishin, and V.A. Saks, *Alterations in the creatine kinase system in the myocardium of cardiomyopathic hamsters.* Biochem Biophys Res Commun, 1989. **165**(2): p. 748-57.
33. Nascimben, L., J. Friedrich, R. Liao, P. Pauletto, A.C. Pessina, and J.S. Ingwall, *Enalapril treatment increases cardiac performance and energy reserve via the creatine kinase reaction in myocardium of Syrian myopathic hamsters with advanced heart failure.* Circulation, 1995. **91**(6): p. 1824-33.
34. Neubauer, S., M. Horn, A. Naumann, R. Tian, K. Hu, M. Laser, J. Friedrich, P. Gaudron, K. Schnackerz, J.S. Ingwall, and et al., *Impairment of energy metabolism in intact residual myocardium of rat hearts with chronic myocardial infarction.* J Clin Invest, 1995. **95**(3): p. 1092-100.

35. Tian, R., L. Nascimben, J.S. Ingwall, and B.H. Lorell, *Failure to maintain a low ADP concentration impairs diastolic function in hypertrophied rat hearts.* Circulation, 1997. **96**(4): p. 1313-9.
36. Smith, C.S., P.A. Bottomley, S.P. Schulman, G. Gerstenblith, and R.G. Weiss, *Altered creatine kinase adenosine triphosphate kinetics in failing hypertrophied human myocardium.* Circulation, 2006. **114**(11): p. 1151-8.
37. Kennel, P.J., D.M. Mancini, and P.C. Schulze, *Skeletal Muscle Changes in Chronic Cardiac Disease and Failure.* Compr Physiol, 2015. **5**(4): p. 1947-69.
38. Wu, F., J. Zhang, and D.A. Beard, *Experimentally observed phenomena on cardiac energetics in heart failure emerge from simulations of cardiac metabolism.* Proc Natl Acad Sci U S A, 2009. **106**(17): p. 7143-8.
39. Sequeira, V., A. Najafi, M. McConnell, E.D. Fowler, I.A. Bollen, R.C. Wust, C. dos Remedios, M. Helmes, E. White, G.J. Stienen, J. Tardiff, D.W. Kuster, and J. van der Velden, *Synergistic role of ADP and Ca(2+) in diastolic myocardial stiffness.* J Physiol, 2015. **593**(17): p. 3899-916.
40. Sequeira, V., A. Najafi, P.J. Wijnker, and C.G. Dos Remedios, *ADP-stimulated contraction: A predictor of thin-filament activation in cardiac disease.* 2015. **112**(50): p. E7003-12.
41. Hiebert, J.B., Q. Shen, A. Thimmesch, and J. Pierce, *Impaired Myocardial Bioenergetics in HFpEF and the Role of Antioxidants.* Open Cardiovasc Med J, 2016. **10**: p. 158-62.
42. Bers, D.M. and T.R. Shannon, *Calcium movements inside the sarcoplasmic reticulum of cardiac myocytes.* J Mol Cell Cardiol, 2013. **58**: p. 59-66.
43. Silberman, G.A., T.H. Fan, H. Liu, Z. Jiao, H.D. Xiao, J.D. Lovelock, B.M. Boulden, J. Widder, S. Fredd, K.E. Bernstein, B.M. Wolska, S. Dikalov, D.G. Harrison, and S.C. Dudley, Jr., *Uncoupled cardiac nitric oxide synthase mediates diastolic dysfunction.* Circulation, 2010. **121**(4): p. 519-28.
44. Moslehi, J., R.A. DePinho, and E. Sahin, *Telomeres and mitochondria in the aging heart.* Circ Res, 2012. **110**(9): p. 1226-37.
45. Birks, E.J., *Molecular changes after left ventricular assist device support for heart failure.* Circ Res, 2013. **113**(6): p. 777-91.
46. Gruson, D., S.A. Ahn, and M.F. Rousseau, *Biomarkers of inflammation and cardiac remodeling: the quest of relevant companions for the risk stratification of heart failure patients is still ongoing.* Biochem Med (Zagreb), 2011. **21**(3): p. 254-63.
47. Schwartz, A. and K.S. Lee, *Study of heart mitochondria and glycolytic metabolism in experimentally induced cardiac failure.* Circ Res, 1962. **10**: p. 321-32.
48. Bugger, H., M. Schwarzer, D. Chen, A. Schrepper, P.A. Amorim, M. Schoepe, T.D. Nguyen, F.W. Mohr, O. Khalimonchuk, B.C. Weimer, and T. Doenst, *Proteomic remodelling of mitochondrial oxidative pathways in pressure overload-induced heart failure.* Cardiovasc Res, 2010. **85**(2): p. 376-84.
49. Liem, D.A., A. Nsair, S.P. Setty, M. Cadeiras, D. Wang, R. Maclellan, C. Lotz, A.J. Lin, J. Tabaraki, H. Li, J. Ge, J. Odeberg, F. Ponten, E. Larson, J. Mulder, E. Lundberg, J.N. Weiss, M. Uhlen, P. Ping, and M.C. Deng, *Molecular- and organelle-based predictive paradigm underlying recovery by left ventricular assist device support.* Circ Heart Fail, 2014. **7**(2): p. 359-66.
50. Sanbe, A., K. Tanonaka, R. Kobayasi, and S. Takeo, *Effects of long-term therapy with ACE inhibitors, captopril, enalapril and trandolapril, on myocardial energy metabolism in rats with heart failure following myocardial infarction.* J Mol Cell Cardiol, 1995. **27**(10): p. 2209-22.
51. Ide, T., H. Tsutsui, S. Hayashidani, D. Kang, N. Suematsu, K. Nakamura, H. Utsumi, N. Hamasaki, and A. Takeshita, *Mitochondrial DNA damage and dysfunction associated with oxidative stress in failing hearts after myocardial infarction.* Circ Res, 2001. **88**(5): p. 529-35.

52. Graff, C., D.A. Clayton, and N.G. Larsson, *Mitochondrial medicine--recent advances.* J Intern Med, 1999. **246**(1): p. 11-23.
53. Pisano, A., B. Cerbelli, E. Perli, M. Pelullo, V. Bargelli, C. Preziuso, M. Mancini, L. He, M.G. Bates, J.R. Lucena, P.L. Della Monica, G. Familiari, V. Petrozza, C. Nediani, R.W. Taylor, G. d'Amati, and C. Giordano, *Impaired mitochondrial biogenesis is a common feature to myocardial hypertrophy and end-stage ischemic heart failure.* Cardiovasc Pathol, 2016. **25**(2): p. 103-12.
54. Dai, D.F., S.C. Johnson, J.J. Villarin, M.T. Chin, M. Nieves-Cintron, T. Chen, D.J. Marcinek, G.W. Dorn, 2nd, Y.J. Kang, T.A. Prolla, L.F. Santana, and P.S. Rabinovitch, *Mitochondrial oxidative stress mediates angiotensin II-induced cardiac hypertrophy and Galphaq overexpression-induced heart failure.* Circ Res, 2011. **108**(7): p. 837-46.
55. Matlib, M.A., J.C. Rembert, R.W. Millard, M. Ashraf, W. Rouslin, G. Asano, J.C. Greenfield, Jr., and A. Schwartz, *Mitochondrial function in canine experimental cardiac hypertrophy.* J Mol Cell Cardiol, 1983. **15**(4): p. 221-32.
56. Echtay, K.S., *Mitochondrial uncoupling proteins--what is their physiological role?* Free Radic Biol Med, 2007. **43**(10): p. 1351-71.
57. Murray, A.J., M.A. Cole, C.A. Lygate, C.A. Carr, D.J. Stuckey, S.E. Little, S. Neubauer, and K. Clarke, *Increased mitochondrial uncoupling proteins, respiratory uncoupling and decreased efficiency in the chronically infarcted rat heart.* J Mol Cell Cardiol, 2008. **44**(4): p. 694-700.
58. Negi, S.I., E.M. Jeong, I. Shukrullah, E. Veleder, D.P. Jones, T.H. Fan, S. Varadarajan, S.M. Danilov, T. Fukai, and S.C. Dudley, Jr., *Renin-Angiotensin Activation and Oxidative Stress in Early Heart Failure with Preserved Ejection Fraction.* Biomed Res Int, 2015. **2015**: p. 825027.
59. Brown, G.C. and V. Borutaite, *Nitric oxide and mitochondrial respiration in the heart.* Cardiovasc Res, 2007. **75**(2): p. 283-90.
60. Mital, S., K.E. Loke, L.J. Addonizio, M.C. Oz, and T.H. Hintze, *Left ventricular assist device implantation augments nitric oxide dependent control of mitochondrial respiration in failing human hearts.* J Am Coll Cardiol, 2000. **36**(6): p. 1897-902.
61. Brown, G.C. and V. Borutaite, *Nitric oxide inhibition of mitochondrial respiration and its role in cell death.* Free Radic Biol Med, 2002. **33**(11): p. 1440-50.
62. Brown, G.C., *Nitric oxide and mitochondrial respiration.* Biochim Biophys Acta, 1999. **1411**(2-3): p. 351-69.
63. Brookes, P.S., J. Zhang, L. Dai, F. Zhou, D.A. Parks, V.M. Darley-Usmar, and P.G. Anderson, *Increased sensitivity of mitochondrial respiration to inhibition by nitric oxide in cardiac hypertrophy.* J Mol Cell Cardiol, 2001. **33**(1): p. 69-82.
64. Kohr, M.J., J.P. Davis, and M.T. Ziolo, *Peroxynitrite Increases Protein Phosphatase Activity and Promotes the Interaction of Phospholamban with Protein Phosphatase 2a in the Myocardium.* Nitric Oxide, 2009. **20**(3): p. 217-221.
65. Paulus, W.J., P.J. Vantrimpont, and A.M. Shah, *Acute effects of nitric oxide on left ventricular relaxation and diastolic distensibility in humans. Assessment by bicoronary sodium nitroprusside infusion.* Circulation, 1994. **89**(5): p. 2070-8.
66. Layland, J., J.M. Li, and A.M. Shah, *Role of cyclic GMP-dependent protein kinase in the contractile response to exogenous nitric oxide in rat cardiac myocytes.* J Physiol, 2002. **540**(Pt 2): p. 457-67.
67. Takimoto, E., *Cyclic GMP-dependent signaling in cardiac myocytes.* Circ J, 2012. **76**(8): p. 1819-25.
68. Hamdani, N., C. Franssen, A. Lourenco, I. Falcao-Pires, D. Fontoura, S. Leite, L. Plettig, B. Lopez, C.A. Ottenheijm, P.M. Becher, A. Gonzalez, C. Tschope, J. Diez, W.A. Linke, A.F. Leite-Moreira, and W.J. Paulus, *Myocardial titin hypophosphorylation importantly contributes to heart failure with preserved ejection fraction in a rat metabolic risk model.* Circ Heart Fail, 2013. **6**(6): p. 1239-49.

69. Grutzner, A., S. Garcia-Manyes, S. Kotter, C.L. Badilla, J.M. Fernandez, and W.A. Linke, *Modulation of titin-based stiffness by disulfide bonding in the cardiac titin N2-B unique sequence.* Biophys J, 2009. **97**(3): p. 825-34.
70. Szelenyi, Z., A. Fazakas, G. Szenasi, M. Kiss, N. Tegze, B.C. Fekete, E. Nagy, I. Bodo, B. Nagy, A. Molvarec, A. Patocs, L. Pepo, Z. Prohaszka, and A. Vereckei, *Inflammation and oxidative stress caused by nitric oxide synthase uncoupling might lead to left ventricular diastolic and systolic dysfunction in patients with hypertension.* J Geriatr Cardiol, 2015. **12**(1): p. 1-10.
71. van Empel, V. and H.P. Brunner-La Rocca, *Inflammation in HFpEF: Key or circumstantial?* Int J Cardiol, 2015. **189**: p. 259-63.
72. Farrar, E.J., G.D. Huntley, and J. Butcher, *Endothelial-derived oxidative stress drives myofibroblastic activation and calcification of the aortic valve.* PLoS One, 2015. **10**(4): p. e0123257.
73. Zhao, W., T. Zhao, Y. Chen, R.A. Ahokas, and Y. Sun, *Oxidative stress mediates cardiac fibrosis by enhancing transforming growth factor-beta1 in hypertensive rats.* Mol Cell Biochem, 2008. **317**(1-2): p. 43-50.
74. Kuwahara, F., H. Kai, K. Tokuda, M. Kai, A. Takeshita, K. Egashira, and T. Imaizumi, *Transforming growth factor-beta function blocking prevents myocardial fibrosis and diastolic dysfunction in pressure-overloaded rats.* Circulation, 2002. **106**(1): p. 130-5.
75. Kasner, M., D. Westermann, B. Lopez, R. Gaub, F. Escher, U. Kuhl, H.P. Schultheiss, and C. Tschope, *Diastolic tissue Doppler indexes correlate with the degree of collagen expression and cross-linking in heart failure and normal ejection fraction.* J Am Coll Cardiol, 2011. **57**(8): p. 977-85.
76. Rodrigues, P.G., A.F. Leite-Moreira, and I. Falcao-Pires, *Myocardial reverse remodeling: how far can we rewind?* 2016. **310**(11): p. H1402-22.
77. Ahmed, S.H., L.L. Clark, W.R. Pennington, C.S. Webb, D.D. Bonnema, A.H. Leonardi, C.D. McClure, F.G. Spinale, and M.R. Zile, *Matrix metalloproteinases/tissue inhibitors of metalloproteinases: relationship between changes in proteolytic determinants of matrix composition and structural, functional, and clinical manifestations of hypertensive heart disease.* Circulation, 2006. **113**(17): p. 2089-96.
78. Haykowsky, M.J., P.H. Brubaker, J.M. John, K.P. Stewart, T.M. Morgan, and D.W. Kitzman, *Determinants of exercise intolerance in elderly heart failure patients with preserved ejection fraction.* J Am Coll Cardiol, 2011. **58**(3): p. 265-74.
79. Bhella, P.S., A. Prasad, K. Heinicke, J.L. Hastings, A. Arbab-Zadeh, B. Adams-Huet, E.L. Pacini, S. Shibata, M.D. Palmer, B.R. Newcomer, and B.D. Levine, *Abnormal haemodynamic response to exercise in heart failure with preserved ejection fraction.* Eur J Heart Fail, 2011. **13**(12): p. 1296-304.
80. Haykowsky, M., P. Brubaker, and D. Kitzman, *Role of physical training in heart failure with preserved ejection fraction.* Curr Heart Fail Rep, 2012. **9**(2): p. 101-6.
81. Dhakal, B.P., R. Malhotra, R.M. Murphy, P.P. Pappagianopoulos, A.L. Baggish, R.B. Weiner, N.E. Houstis, A.S. Eisman, S.S. Hough, and G.D. Lewis, *Mechanisms of exercise intolerance in heart failure with preserved ejection fraction: the role of abnormal peripheral oxygen extraction.* Circ Heart Fail, 2015. **8**(2): p. 286-94.
82. Borlaug, B.A., V. Melenovsky, S.D. Russell, K. Kessler, K. Pacak, L.C. Becker, and D.A. Kass, *Impaired chronotropic and vasodilator reserves limit exercise capacity in patients with heart failure and a preserved ejection fraction.* Circulation, 2006. **114**(20): p. 2138-47.
83. Borlaug, B.A., T.P. Olson, C.S. Lam, K.S. Flood, A. Lerman, B.D. Johnson, and M.M. Redfield, *Global cardiovascular reserve dysfunction in heart failure with preserved ejection fraction.* J Am Coll Cardiol, 2010. **56**(11): p. 845-54.
84. Kawaguchi, M., I. Hay, B. Fetics, and D.A. Kass, *Combined ventricular systolic and arterial stiffening in patients with heart failure and preserved ejection fraction:*

implications for systolic and diastolic reserve limitations. Circulation, 2003. **107**(5): p. 714-20.
85. Mohammed, S.F., S. Hussain, S.A. Mirzoyev, W.D. Edwards, J.J. Maleszewski, and M.M. Redfield, *Coronary microvascular rarefaction and myocardial fibrosis in heart failure with preserved ejection fraction.* Circulation, 2015. **131**(6): p. 550-9.
86. Abudiab, M.M., M.M. Redfield, V. Melenovsky, T.P. Olson, D.A. Kass, B.D. Johnson, and B.A. Borlaug, *Cardiac output response to exercise in relation to metabolic demand in heart failure with preserved ejection fraction.* Eur J Heart Fail, 2013. **15**(7): p. 776-85.
87. Kitzman, D.W., B. Nicklas, W.E. Kraus, M.F. Lyles, J. Eggebeen, T.M. Morgan, and M. Haykowsky, *Skeletal muscle abnormalities and exercise intolerance in older patients with heart failure and preserved ejection fraction.* Am J Physiol Heart Circ Physiol, 2014. **306**(9): p. H1364-70.
88. Bowen, T.S., N.P. Rolim, T. Fischer, F.H. Baekkerud, A. Medeiros, S. Werner, E. Bronstad, O. Rognmo, N. Mangner, A. Linke, G. Schuler, G.J. Silva, U. Wisloff, V. Adams, and G. Optimex Study, *Heart failure with preserved ejection fraction induces molecular, mitochondrial, histological, and functional alterations in rat respiratory and limb skeletal muscle.* Eur J Heart Fail, 2015. **17**(3): p. 263-72.
89. Molina, A.J., M.S. Bharadwaj, C. Van Horn, B.J. Nicklas, M.F. Lyles, J. Eggebeen, M.J. Haykowsky, P.H. Brubaker, and D.W. Kitzman, *Skeletal Muscle Mitochondrial Content, Oxidative Capacity, and Mfn2 Expression Are Reduced in Older Patients With Heart Failure and Preserved Ejection Fraction and Are Related to Exercise Intolerance.* JACC Heart Fail, 2016. **4**(8): p. 636-45.
90. Kass, D.A., K.L. Baughman, P.H. Pak, P.W. Cho, H.R. Levin, T.J. Gardner, H.R. Halperin, J.E. Tsitlik, and M.A. Acker, *Reverse remodeling from cardiomyoplasty in human heart failure. External constraint versus active assist.* Circulation, 1995. **91**(9): p. 2314-8.
91. Zaid, R.R., C.M. Barker, S.H. Little, and S.F. Nagueh, *Pre- and post-operative diastolic dysfunction in patients with valvular heart disease: diagnosis and therapeutic implications.* J Am Coll Cardiol, 2013. **62**(21): p. 1922-30.
92. Biederman, R.W., J.A. Magovern, S.B. Grant, R.B. Williams, J.A. Yamrozik, D.A. Vido, V.K. Rathi, G. Rayarao, K. Caruppannan, and M. Doyle, *LV reverse remodeling imparted by aortic valve replacement for severe aortic stenosis; is it durable? A cardiovascular MRI study sponsored by the American Heart Association.* J Cardiothorac Surg, 2011. **6**: p. 53.
93. Blair, J.E.A., P. Atri, J.L. Friedman, J.D. Thomas, K. Brummel, R.N. Sweis, I. Mikati, S.C. Malaisrie, C.J. Davidson, and J.D. Flaherty, *Diastolic Function and Transcatheter Aortic Valve Replacement.* J Am Soc Echocardiogr, 2017. **30**(6): p. 541-551.
94. Ruppert, M., S. Korkmaz-Icoz, S. Li, B.T. Nemeth, P. Hegedus, P. Brlecic, C. Matyas, M. Zorn, B. Merkely, M. Karck, T. Radovits, and G. Szabo, *Myocardial reverse remodeling after pressure unloading is associated with maintained cardiac mechanoenergetics in a rat model of left ventricular hypertrophy.* Am J Physiol Heart Circ Physiol, 2016. **311**(3): p. H592-603.
95. Gallet, R., G. de Couto, E. Simsolo, J. Valle, B. Sun, W. Liu, E. Tseliou, M.R. Zile, and E. Marban, *Cardiosphere-derived cells reverse heart failure with preserved ejection fraction (HFpEF) in rats by decreasing fibrosis and inflammation.* JACC Basic Transl Sci, 2016. **1**(1-2): p. 14-28.
96. Gupte, A.A., D.J. Hamilton, A.M. Cordero-Reyes, K.A. Youker, Z. Yin, J.D. Estep, R.D. Stevens, B. Wenner, O. Ilkayeva, M. Loebe, L.E. Peterson, C.J. Lyon, S.T. Wong, C.B. Newgard, G. Torre-Amione, H. Taegtmeyer, and W.A. Hsueh, *Mechanical unloading promotes myocardial energy recovery in human heart failure.* Circ Cardiovasc Genet, 2014. **7**(3): p. 266-76.
97. Lee, J., S. Giordano, and J. Zhang, *Autophagy, mitochondria and oxidative stress: cross-talk and redox signalling.* Biochem J, 2012. **441**(2): p. 523-40.
98. de Jonge, N., H. Kirkels, J.R. Lahpor, C. Klopping, E.J. Hulzebos, A.B. de la Riviere, and E.O. Robles de Medina, *Exercise performance in patients with end-stage heart failure after*

implantation of a left ventricular assist device and after heart transplantation: an outlook for permanent assisting? J Am Coll Cardiol, 2001. **37**(7): p. 1794-9.
99. Mondal, N.K., E. Sorensen, N. Hiivala, E. Feller, B. Griffith, and Z.J. Wu, *Oxidative stress, DNA damage and repair in heart failure patients after implantation of continuous flow left ventricular assist devices.* Int J Med Sci, 2013. **10**(7): p. 883-93.
100. Mondal, N.K., E.N. Sorensen, S.M. Pham, S.C. Koenig, B.P. Griffith, M.S. Slaughter, and Z.J. Wu, *Systemic Inflammatory Response Syndrome in End-Stage Heart Failure Patients Following Continuous-Flow Left Ventricular Assist Device Implantation: Differences in Plasma Redox Status and Leukocyte Activation.* Artif Organs, 2016. **40**(5): p. 434-43.
101. Nishimura, M., B. Radovancevic, P. Odegaard, T. Myers, W. Springer, and O.H. Frazier, *Exercise capacity recovers slowly but fully in patients with a left ventricular assist device.* Asaio j, 1996. **42**(5): p. M568-70.
102. Van Norman, K.H., *The Biuret Reaction and the Cold Nitric Acid Test in the Recognition of Protein.* Biochem J, 1909. **4**(3-4): p. 127-35.
103. Maitra, P.K. and R.W. Estabrook, *Studies of baker's yeast metabolism. II. The role of adenine nucleotides and inorganic phosphate in the control of respiration during alcohol oxidation.* Arch Biochem Biophys, 1967. **121**(1): p. 129-39.
104. Ascensao, A., J. Lumini-Oliveira, N.G. Machado, R.M. Ferreira, I.O. Goncalves, A.C. Moreira, F. Marques, V.A. Sardao, P.J. Oliveira, and J. Magalhaes, *Acute exercise protects against calcium-induced cardiac mitochondrial permeability transition pore opening in doxorubicin-treated rats.* Clin Sci (Lond), 2011. **120**(1): p. 37-49.
105. Kamo, N., M. Muratsugu, R. Hongoh, and Y. Kobatake, *Membrane potential of mitochondria measured with an electrode sensitive to tetraphenyl phosphonium and relationship between proton electrochemical potential and phosphorylation potential in steady state.* J Membr Biol, 1979. **49**(2): p. 105-21.
106. Goncalves, N., A.F. Silva, P.G. Rodrigues, E. Correia, C. Moura, C. Eloy, R. Roncon-Albuquerque, Jr., I. Falcao-Pires, and A.F. Leite-Moreira, *Early cardiac changes induced by a hypercaloric Western-type diet in "subclinical" obesity.* Am J Physiol Heart Circ Physiol, 2016. **310**(6): p. H655-66.
107. Melenovsky, V., B.A. Borlaug, B. Rosen, I. Hay, L. Ferruci, C.H. Morell, E.G. Lakatta, S.S. Najjar, and D.A. Kass, *Cardiovascular features of heart failure with preserved ejection fraction versus nonfailing hypertensive left ventricular hypertrophy in the urban Baltimore community: the role of atrial remodeling/dysfunction.* J Am Coll Cardiol, 2007. **49**(2): p. 198-207.
108. Dai, J., D.F. Shen, Z.Y. Bian, H. Zhou, H.W. Gan, J. Zong, W. Deng, Y. Yuan, F. Li, Q.Q. Wu, L. Gao, R. Zhang, Z.G. Ma, H.L. Li, and Q.Z. Tang, *IKKi deficiency promotes pressure overload-induced cardiac hypertrophy and fibrosis.* PLoS One, 2013. **8**(1): p. e53412.
109. Sugden, P.H., S.J. Fuller, S.C. Weiss, and A. Clerk, *Glycogen synthase kinase 3 (GSK3) in the heart: a point of integration in hypertrophic signalling and a therapeutic target? A critical analysis.* Br J Pharmacol, 2008. **153 Suppl 1**: p. S137-53.
110. Hudson, B., C. Hidalgo, C. Saripalli, and H. Granzier, *Hyperphosphorylation of mouse cardiac titin contributes to transverse aortic constriction-induced diastolic dysfunction.* Circ Res, 2011. **109**(8): p. 858-66.
111. Franssen, C., S. Chen, A. Unger, H.I. Korkmaz, G.W. De Keulenaer, C. Tschope, A.F. Leite-Moreira, R. Musters, H.W. Niessen, W.A. Linke, W.J. Paulus, and N. Hamdani, *Myocardial Microvascular Inflammatory Endothelial Activation in Heart Failure With Preserved Ejection Fraction.* JACC Heart Fail, 2016. **4**(4): p. 312-24.
112. Falcao-Pires, I., G. Palladini, N. Goncalves, J. van der Velden, D. Moreira-Goncalves, D. Miranda-Silva, F. Salinaro, W.J. Paulus, H.W. Niessen, S. Perlini, and A.F. Leite-Moreira, *Distinct mechanisms for diastolic dysfunction in diabetes mellitus and chronic pressure-overload.* Basic Res Cardiol, 2011. **106**(5): p. 801-14.

113. Rose, A.G. and S.J. Park, *Pathology in patients with ventricular assist devices: a study of 21 autopsies, 24 ventricular apical core biopsies and 24 explanted hearts.* Cardiovasc Pathol, 2005. **14**(1): p. 19-23.
114. Chen, Y., H. Guo, D. Xu, X. Xu, H. Wang, X. Hu, Z. Lu, D. Kwak, Y. Xu, R. Gunther, Y. Huo, and E.K. Weir, *Left ventricular failure produces profound lung remodeling and pulmonary hypertension in mice: heart failure causes severe lung disease.* Hypertension, 2012. **59**(6): p. 1170-8.
115. Adeniran, I., D.H. MacIver, J.C. Hancox, and H. Zhang, *Abnormal calcium homeostasis in heart failure with preserved ejection fraction is related to both reduced contractile function and incomplete relaxation: an electromechanically detailed biophysical modeling study.* Front Physiol, 2015. **6**: p. 78.
116. Sande, J.B., I. Sjaastad, I.B. Hoen, J. Bokenes, T. Tonnessen, E. Holt, P.K. Lunde, and G. Christensen, *Reduced level of serine(16) phosphorylated phospholamban in the failing rat myocardium: a major contributor to reduced SERCA2 activity.* Cardiovasc Res, 2002. **53**(2): p. 382-91.
117. Moens, A.L., E. Takimoto, C.G. Tocchetti, K. Chakir, D. Bedja, G. Cormaci, E.A. Ketner, M. Majmudar, K. Gabrielson, M.K. Halushka, J.B. Mitchell, S. Biswal, K.M. Channon, M.S. Wolin, N.J. Alp, N. Paolocci, H.C. Champion, and D.A. Kass, *Reversal of cardiac hypertrophy and fibrosis from pressure overload by tetrahydrobiopterin: efficacy of recoupling nitric oxide synthase as a therapeutic strategy.* Circulation, 2008. **117**(20): p. 2626-36.
118. Macdonald, P., C. Schyvens, and D. Winlaw, *The role of nitric oxide in heart failure. Potential for pharmacological intervention.* Drugs Aging, 1996. **8**(6): p. 452-8.
119. Soskic, S.S., B.D. Dobutovic, E.M. Sudar, M.M. Obradovic, D.M. Nikolic, J.D. Djordjevic, D.J. Radak, D.P. Mikhailidis, and E.R. Isenovic, *Regulation of Inducible Nitric Oxide Synthase (iNOS) and its Potential Role in Insulin Resistance, Diabetes and Heart Failure.* Open Cardiovasc Med J, 2011. **5**: p. 153-63.
120. Zhang, P., X. Xu, X. Hu, E.D. van Deel, G. Zhu, and Y. Chen, *Inducible nitric oxide synthase deficiency protects the heart from systolic overload-induced ventricular hypertrophy and congestive heart failure.* Circ Res, 2007. **100**(7): p. 1089-98.
121. Bhushan, S., K. Kondo, D.J. Polhemus, H. Otsuka, C.K. Nicholson, Y.X. Tao, H. Huang, V.V. Georgiopoulou, T. Murohara, J.W. Calvert, J. Butler, and D.J. Lefer, *Nitrite therapy improves left ventricular function during heart failure via restoration of nitric oxide-mediated cytoprotective signaling.* Circ Res, 2014. **114**(8): p. 1281-91.
122. Velez Rueda, J.O., J. Palomeque, and A. Mattiazzi, *Early apoptosis in different models of cardiac hypertrophy induced by high renin-angiotensin system activity involves CaMKII.* J Appl Physiol (1985), 2012. **112**(12): p. 2110-20.
123. Bao, W., D.J. Behm, S.S. Nerurkar, Z. Ao, R. Bentley, R.C. Mirabile, D.G. Johns, T.N. Woods, C.P. Doe, R.W. Coatney, J.F. Ohlstein, S.A. Douglas, R.N. Willette, and T.L. Yue, *Effects of p38 MAPK Inhibitor on angiotensin II-dependent hypertension, organ damage, and superoxide anion production.* J Cardiovasc Pharmacol, 2007. **49**(6): p. 362-8.
124. Cai, B., S.H. Chang, E.B. Becker, A. Bonni, and Z. Xia, *p38 MAP kinase mediates apoptosis through phosphorylation of BimEL at Ser-65.* J Biol Chem, 2006. **281**(35): p. 25215-22.
125. Moorjani, N., M. Ahmad, P. Catarino, R. Brittin, D. Trabzuni, F. Al-Mohanna, N. Narula, J. Narula, and S. Westaby, *Activation of apoptotic caspase cascade during the transition to pressure overload-induced heart failure.* J Am Coll Cardiol, 2006. **48**(7): p. 1451-8.
126. Liu, T., L. Chen, E. Kim, D. Tran, B.S. Phinney, and A.A. Knowlton, *Mitochondrial proteome remodeling in ischemic heart failure.* Life Sci, 2014. **101**(1-2): p. 27-36.
127. Chen, H., S.A. Detmer, A.J. Ewald, E.E. Griffin, S.E. Fraser, and D.C. Chan, *Mitofusins Mfn1 and Mfn2 coordinately regulate mitochondrial fusion and are essential for embryonic development.* J Cell Biol, 2003. **160**(2): p. 189-200.

128. Naon, D., M. Zaninello, M. Giacomello, T. Varanita, F. Grespi, S. Lakshminaranayan, A. Serafini, M. Semenzato, S. Herkenne, M.I. Hernandez-Alvarez, A. Zorzano, D. De Stefani, G.W. Dorn, 2nd, and L. Scorrano, *Critical reappraisal confirms that Mitofusin 2 is an endoplasmic reticulum-mitochondria tether.* Proc Natl Acad Sci U S A, 2016. **113**(40): p. 11249-11254.
129. Fearnley, C.J., H.L. Roderick, and M.D. Bootman, *Calcium signaling in cardiac myocytes.* Cold Spring Harb Perspect Biol, 2011. **3**(11): p. a004242.
130. Rosca, M.G., B. Tandler, and C.L. Hoppel, *Mitochondria in cardiac hypertrophy and heart failure.* J Mol Cell Cardiol, 2013. **55**: p. 31-41.
131. Mei, Z., X. Wang, W. Liu, J. Gong, X. Gao, T. Zhang, F. Xie, and L. Qian, *Mitochondrial adaptations during myocardial hypertrophy induced by abdominal aortic constriction.* Cardiovasc Pathol, 2014. **23**(5): p. 283-8.
132. Lindenmayer, G.E., L.A. Sordahl, S. Harigaya, J.C. Allen, H.R. Besch, Jr., and A. Schwartz, *Some biochemical studies on subcellular systems isolated from fresh recipient human cardiac tissue obtained during transplantation.* Am J Cardiol, 1971. **27**(3): p. 277-83.
133. Sordahl, L.A., W.B. McCollum, W.G. Wood, and A. Schwartz, *Mitochondria and sarcoplasmic reticulum function in cardiac hypertrophy and failure.* Am J Physiol, 1973. **224**(3): p. 497-502.
134. Doenst, T., G. Pytel, A. Schrepper, P. Amorim, G. Farber, Y. Shingu, F.W. Mohr, and M. Schwarzer, *Decreased rates of substrate oxidation ex vivo predict the onset of heart failure and contractile dysfunction in rats with pressure overload.* Cardiovasc Res, 2010. **86**(3): p. 461-70.
135. Shao, D. and R. Tian, *Glucose Transporters in Cardiac Metabolism and Hypertrophy.* Compr Physiol, 2015. **6**(1): p. 331-51.
136. Kolwicz, S.C., Jr. and R. Tian, *Glucose metabolism and cardiac hypertrophy.* Cardiovasc Res, 2011. **90**(2): p. 194-201.
137. Zhang, S., M.W. Hulver, R.P. McMillan, M.A. Cline, and E.R. Gilbert, *The pivotal role of pyruvate dehydrogenase kinases in metabolic flexibility.* Nutr Metab (Lond), 2014. **11**(1): p. 10.
138. Kamga, C., S. Krishnamurthy, and S. Shiva, *Myoglobin and mitochondria: a relationship bound by oxygen and nitric oxide.* Nitric Oxide, 2012. **26**(4): p. 251-8.
139. Brand, M.D. and D.G. Nicholls, *Assessing mitochondrial dysfunction in cells.* Biochem J, 2011. **435**(2): p. 297-312.
140. Cabrera, J.A., E.A. Ziemba, R. Colbert, R.F. Kelly, M. Kuskowski, E.A. Arriaga, W. Sluiter, D.J. Duncker, H.B. Ward, and E.O. McFalls, *Uncoupling protein-2 expression and effects on mitochondrial membrane potential and oxidant stress in heart tissue.* Transl Res, 2012. **159**(5): p. 383-90.
141. Havlickova Karbanova, V., A. Cizkova Vrbacka, K. Hejzlarova, H. Nuskova, V. Stranecky, A. Potocka, S. Kmoch, and J. Houstek, *Compensatory upregulation of respiratory chain complexes III and IV in isolated deficiency of ATP synthase due to TMEM70 mutation.* Biochim Biophys Acta, 2012. **1817**(7): p. 1037-43.
142. Pennanen, C., V. Parra, C. Lopez-Crisosto, P.E. Morales, A. Del Campo, T. Gutierrez, P. Rivera-Mejias, J. Kuzmicic, M. Chiong, A. Zorzano, B.A. Rothermel, and S. Lavandero, *Mitochondrial fission is required for cardiomyocyte hypertrophy mediated by a Ca2+-calcineurin signaling pathway.* J Cell Sci, 2014. **127**(Pt 12): p. 2659-71.
143. Nagendran, J., V. Gurtu, D.Z. Fu, J.R. Dyck, A. Haromy, D.B. Ross, I.M. Rebeyka, and E.D. Michelakis, *A dynamic and chamber-specific mitochondrial remodeling in right ventricular hypertrophy can be therapeutically targeted.* J Thorac Cardiovasc Surg, 2008. **136**(1): p. 168-78, 178 e1-3.
144. Arany, Z., M. Novikov, S. Chin, Y. Ma, A. Rosenzweig, and B.M. Spiegelman, *Transverse aortic constriction leads to accelerated heart failure in mice lacking PPAR-gamma coactivator 1alpha.* Proc Natl Acad Sci U S A, 2006. **103**(26): p. 10086-91.

145. Zizola, C. and P.C. Schulze, *Metabolic and structural impairment of skeletal muscle in heart failure*. Heart Fail Rev, 2013. **18**(5): p. 623-30.